

**THE GASEOUS EXTENT OF GALAXIES AND THE ORIGIN
OF $\text{Ly}\alpha$ ABSORPTION SYSTEMS. V. OPTICAL AND
NEAR-INFRARED PHOTOMETRY OF $\text{Ly}\alpha$ -ABSORBING
GALAXIES AT $z < 1$ ¹**

HSIAO-WEN CHEN^{2,3} and KENNETH M. LANZETTA²

Department of Physics and Astronomy, State University of New York at Stony Brook
Stony Brook, NY 11794-3800, U.S.A.
lanzetta@sbastr.ess.sunysb.edu

JOHN K. WEBB

School of Physics, University of New South Wales
Sydney 2052, NSW, AUSTRALIA
jkw@edwin.phys.unsw.edu.au

and

XAVIER BARCONS

Instituto de Física de Cantabria (Consejo Superior de Investigaciones Científicas—
Universidad de Cantabria)
39005 Santander, SPAIN
barcons@ifca.unican.es

¹Based on observations with the NASA/ESA Hubble Space Telescope, obtained at the Space Telescope Science Institute, which is operated by the Association of Universities for Research in Astronomy, Inc., under NASA contract NAS5-26555.

²Visiting Astronomer at Infrared Telescope Facility, which is operated by the University of Hawaii under contract to the National Aeronautics and Space Administration

³Current address: The Observatories of the Carnegie Institution of Washington, 813 Santa Barbara Street, Pasadena, CA 91101, U.S.A. E-Mail: hchen@ociw.edu

ABSTRACT

We present results of a program to obtain and analyze HST WFPC2 images and ground-based images of galaxies identified in an imaging and spectroscopic survey of faint galaxies in fields of HST spectroscopic target QSOs. Considering a sample of physically correlated galaxy and absorber pairs with galaxy–absorber cross-correlation amplitude $\xi_{\text{ga}}(v, \rho) > 1$ and with galaxy impact parameter $\rho < 200 h^{-1}$ kpc, we confirm and improve the results presented by Lanzetta et al. (1995) and Chen et al. (1998) that (1) extended gaseous envelopes are a common and generic feature of galaxies of a wide range of luminosity and morphological type, (2) the extent of tenuous gas ($N(\text{HI}) \gtrsim 10^{14} \text{ cm}^{-2}$) around galaxies scales with galaxy B -band luminosity as $r \propto L_B^{0.39 \pm 0.09}$, and (3) galaxy interactions do not play an important role in distributing tenuous gas around galaxies in most cases. We further demonstrate that (4) the gaseous extent of galaxies scales with galaxy K -band luminosity as $r \propto L_K^{0.28 \pm 0.08}$, and (5) tenuous gas around typical L_* galaxies is likely to be distributed in spherical halos of radius $\approx 180 h^{-1}$ kpc of covering factor of nearly unity. The sample consists of 34 galaxy and absorber pairs and 13 galaxies that do not produce Ly α absorption lines to within sensitive upper limits. Redshifts of the galaxy and absorber pairs range from $z = 0.0752$ to 0.8920 with a median of $z = 0.3567$; impact parameter separations of the galaxy and absorber pairs range from $\rho = 12.4$ to $175.2 h^{-1}$ kpc with a median of $\rho = 62.2 h^{-1}$ kpc. Of the galaxies, 15 (32%) are of B -band luminosity $L_B < 0.25 L_{B*}$ and six (13%) are of low surface brightness. The galaxy sample is therefore representative of the galaxy population over a large fraction of the Hubble time. Because galaxies of all morphological types possess extended gaseous halos and because the extent of tenuous gas around galaxies scales with galaxy K -band luminosity, we argue that galaxy mass—rather than recent star-formation activity—is likely to be the dominant factor that determines the extent of tenuous gas around galaxies. Nevertheless, applying the scaling relationship between the extent of Ly α absorbing gas around galaxies and galaxy B -band luminosity, the results of our analysis also suggest that the number density evolution of Ly α absorption systems may serve to constrain the evolution of the comoving galaxy B -band luminosity density (at least for the redshift interval between $z \sim 0$ and $z \sim 1$ that has been studied in our survey).

Subject headings: galaxies: evolution—quasars: absorption lines

1. INTRODUCTION

The “forest” of Ly α absorption systems observed in the spectra of background QSOs traces neutral hydrogen gas to redshifts $z \approx 5$. Because galaxies in the local universe possess extended neutral hydrogen gas (e.g. van Gorkom 1993), some fraction of the observed Ly α absorption systems must arise in individual galaxies. Whether or not this is a dominant fraction is crucial for understanding the origin of Ly α absorption systems, and understanding the origin of Ly α absorption systems bears significantly on all efforts to apply the Ly α forest as a probe of tenuous gas around galaxies over the redshift interval probed by the Ly α absorption systems. Over the past decade, comparison of galaxies and Ly α absorption systems along common lines of sight has shown that low-redshift Ly α absorption systems are associated with intervening galaxies (e.g. Morris et al. 1993), but whether these absorbers arise in individual galaxies or merely trace the large-scale galaxy distribution is still a matter of some debate (Lanzetta et al. 1995; Stocke et al. 1995; Bowen, Blades, & Pettini 1996; Le Brun, Bergeron, & Boissé 1996; van Gorkom et al. 1996; Shull, Stocke, & Penton 1996; Tripp, Lu, & Savage 1998; Chen et al. 1998; Impey, Petry, & Flint 1999).

Over the past several years, we have been conducting an imaging and spectroscopic survey of faint galaxies in fields of Hubble Space Telescope (HST) spectroscopic target QSOs (Lanzetta et al. 1995; Lanzetta, Webb, & Barcons 1995, 1996, 1997, 2001; Barcons, Lanzetta, & Webb 1995; Chen et al. 1998). The goal of the survey is to determine the gaseous extent of galaxies and the origin of QSO absorption systems by directly comparing galaxies and QSO absorption systems along common lines of sight. We have so far identified 352 galaxies of apparent magnitude $m_R < 23$ at redshifts $z < 1.2$, and 230 Ly α absorption systems with rest-frame absorption equivalent width $W > 0.09$ and 36 CIV absorption systems with rest-frame absorption equivalent width $W > 0.09$ at redshifts $z < 1.6$ in 24 QSO fields. Impact parameters (i.e. projected distances) of the galaxies to the QSO lines of sight range from $\rho = 10.9 h^{-1}$ kpc to $1576.7 h^{-1}$ kpc. The galaxy and absorber pair sample is therefore unique for studying the relationship between both Ly α and CIV absorption systems and galaxies. In this paper, we address the relationship between Ly α absorption systems and galaxies; we address the relationship between CIV absorption systems and galaxies in a separate paper (Chen, Lanzetta, & Webb 2000).

The first results of the survey presented by Lanzetta et al. (1995) based on 11 galaxy and Ly α absorber pairs and 13 galaxies that do not produce corresponding Ly α absorption lines to within sensitive upper limits in six QSO fields showed that there is a distinct anti-correlation between Ly α absorption equivalent width and galaxy impact parameter, although the scatter about the mean relationship is substantial. This distinct anti-correlation strongly indicates that most luminous galaxies possess extended gaseous envelopes, but the large

scatter about the mean relationship indicates that the gaseous extent of galaxies may depend on other galaxy properties in addition to galaxy impact parameter. To determine how the extent of tenuous gas around galaxies scales with galaxy properties is crucial not only for discriminating among competing models of the origin of tenuous gas (e.g. Rauch 1998 and references therein) but also for applying the statistics of Ly α absorption systems to constrain the statistics of faint galaxies over the redshift interval probed by the Ly α absorption systems.

To address this issue, we have conducted a program to obtain and analyze images of galaxies in 19 QSO fields, using the HST Wide Field and Planetary Camera 2 (WFPC2) with the F702W and F606W filters and the NASA 3 m Infrared Telescope Facility (IRTF) on Mauna Kea with the K' filter. The primary objectives of the program are (1) to study how the incidence and extent of tenuous gas around galaxies depends on galaxy properties, including perhaps galaxy luminosity, size, or morphological type, (2) to study the spatial distribution of extended gas around galaxies, e.g. whether tenuous gas is distributed around galaxies in flattened disks (in which case absorption should occur preferentially in galaxies of low inclination angle) or in spherical halos (in which case absorption should be independent of galaxy inclination and orientation), and (3) to determine whether extended gas around galaxies arises as a result of galaxy interactions, as evidenced by disturbed morphologies or the presence of close companions.

Initial results of the program based on 87 galaxies identified in ten QSO fields have been published by Chen et al. (1998; hereafter Paper I). In that paper, we presented a two-dimensional surface brightness profile analysis of HST WFPC2 images of the galaxies to measure galaxy B -band luminosity, effective radius, mean surface brightness, inclination and orientation of the disk component, axial ratio of the bulge component, and disk-to-bulge ratio. In addition, we presented an anti-correlation analysis to study the dependence of gaseous extent of galaxies on the measurable galaxy parameters. We found that (1) the amount of gas encountered along the line of sight depends on the galaxy impact parameter and B -band luminosity but does not depend strongly on the galaxy mean surface brightness, disk-to-bulge ratio, or redshift, (2) spherical halos cannot be distinguished from flattened disks based on the galaxy and absorber sample, and (3) there is no evidence that galaxy interactions play an important role in distributing tenuous gas around galaxies in most cases. The statistically significant scaling relation between Ly α absorption equivalent width and galaxy luminosity further supported the hypothesis that the absorbers trace tenuous gas in individual halos surrounding the galaxies rather than tenuous gas in galaxy groups or large-scale filaments around the galaxies.

In this paper, we present complete results of the program, including HST WFPC2 photometry for an additional 68 galaxies in the remaining nine QSO fields and near-infrared

photometry for 75 galaxies in 15 of the 19 QSO fields. The new near-infrared galaxy photometry complements the optical galaxy photometry and helps to interpret the results of the anti-correlation analysis, because, while galaxy B -band luminosity is a measure of recent star-forming activity, galaxy K -band luminosity is a more sensitive measure of total stellar mass, which may be a more fundamental factor (in comparison with recent star formation activity) in scaling the extent of tenuous gas around galaxies. By supplementing the optical photometric measurements of the additional galaxies and including near-infrared galaxy photometry, we further examine whether or not the results of previous analysis may be retained and improved.

Comparison of galaxies and absorbers identified in the 19 QSO fields yields 40 galaxies that are associated with corresponding Ly α absorption lines and 47 galaxies that do not produce corresponding Ly α absorption lines to within sensitive upper limits. Galaxy and absorber pairs are considered to be physically correlated if (1) the galaxy–absorber cross-correlation amplitude satisfies $\xi_{\text{ga}}(v, \rho) > 1$ and (2) the galaxy impact parameter satisfies $\rho < 200 h^{-1}$ kpc. Including only galaxy and absorber pairs that are likely to be physically associated and excluding galaxy and absorber pairs within 3000 km s^{-1} of the background QSOs leaves 34 galaxy and absorber pairs and 13 galaxies that do not produce corresponding Ly α absorption lines to within sensitive upper limits. Redshifts of the galaxy and absorber pairs range from $z = 0.0752$ to 0.8920 with a median of $z = 0.3567$, and impact parameter separations of the galaxy and absorber pairs range from $\rho = 12.4$ to $175.2 h^{-1}$ kpc with a median of $\rho = 62.2 h^{-1}$ kpc. Of the 47 galaxies, 15 (32%) are of B -band luminosity $L_B < 0.25 L_{B*}$ with redshifts ranging from $z = 0.0915$ to 0.6350 , and six (13%) are of low surface brightness with redshifts ranging from $z = 0.0915$ to 0.3180 . The galaxy sample is therefore representative of the galaxy population over a large fraction of the Hubble time.

Based on the new larger galaxy and absorber pair sample, we confirm that the amount of gas encountered along the line of sight depends on the galaxy impact parameter and B -band luminosity but does not depend strongly on the galaxy mean surface brightness, disk-to-bulge ratio, or redshift. In addition, we find that (1) the gaseous extent of galaxies scales with galaxy K -band luminosity as $r \propto L_K^{0.28 \pm 0.08}$, (2) tenuous gas is more likely to be distributed in spherical halos than in flattened disks, and (3) typical L_* galaxies are surrounded by extended gas of radius $\approx 180 h^{-1}$ kpc and covering factor (within $180 h^{-1}$ kpc) of $\approx 94\%$. Because galaxies of all morphological types possess extended gaseous halos and because the extent of tenuous gas around galaxies scales with galaxy K -band luminosity, we conclude that galaxy mass—rather than recent star-formation activity—is likely to be the dominant factor that determines the extent of tenuous gas around galaxies. But because galaxy K -band luminosity is strongly correlated with galaxy B -band luminosity (at least for galaxies at redshifts $z < 1$), we also demonstrate on the basis of the scaling relation

between the extent of Ly α absorbing gas around galaxies and galaxy B -band luminosity that the number density evolution of Ly α absorption systems may serve to constrain the measurements of the cosmic star formation rate density. We adopt a standard Friedmann cosmology of dimensionless Hubble constant $h = H_0/(100 \text{ km s}^{-1} \text{ Mpc}^{-1})$ and deceleration parameter $q_0 = 0.5$ throughout this paper.

2. OBSERVATIONS

In this section, we describe the additional HST WFPC2 observations of galaxies in ten QSO fields that were not included in Paper I and near-infrared imaging observations of galaxies in 15 QSO fields.

2.1. WFPC2 Imaging Observations

Imaging observations of the fields surrounding 0122–0021, 0405–1219 (covering different pointings), 0903+1658, 1136–1334, 1216+0657, 1259+5920, 1424–1150, 1641+3954, and 2251+1552 were obtained with HST using WFPC2 with the F702W filter in Cycle 6. The observations were obtained in a series of three exposures of 700 s each. The journal of observations is given in Table 1, which lists the field, 2000 coordinates α and δ of the QSO, emission redshift z_{em} of the QSO, filter, exposure time, and date of observation.

Imaging observations of objects in the fields surrounding 1317+2743 were accessed from the HST archive. The observations were obtained with the HST using WFPC2 with the F702W filter. The observations were carried out in a series of four exposures of between 1000 and 1300 s each. The journal of archival observations is given in Table 2, which lists the field, 2000 coordinates α and δ of the QSO, emission redshift z_{em} of the QSO, filter, exposure time, and date of observation.

All the images were processed following the prescriptions described in Paper I. The spatial resolution of the final images was measured to be FWHM ≈ 0.1 arcsec, and the 5σ point-source detection thresholds of unresolved objects were measured to span the range $m = 26.2$ through $m = 27.0$.

2.2. Near-infrared Imaging Observations

Near-infrared imaging observations of objects in the fields 0122–0021, 0349–1438, 0405–1219, 0454–2203, 0850+4400, 0903+1658, 1001+2910, 1136–1334, 1216+0657, 1259+5920, 1354+1933, 1424–1150, 1545+2101, 1704+6048, and 2251+1552 were obtained using the IRTF 3 m telescope with the NSFCAM and the K' filter in April and October 1998. The observations were carried out in a series of nine exposures dithered by between ≈ 7 and 20 arcsec in space to remove hot pixels. Individual exposures were flat fielded using a “sliding flat” determined from the median image of nine adjacent frames, registered to a common origin using stars or the QSOs, and coadded using a proper weight determined from the sky variance to form final combined images. A 1σ error image was formed simultaneously for each combined image through appropriate error propagations. The total exposure time of each pointing was approximately 1620 s. The spatial resolutions of the final combined images were measured to span from FWHM ≈ 0.6 to ≈ 1.0 arcsec, and the 5σ point-source detection thresholds were measured to vary from $m = 21.5$ to $m = 22.2$.

2.3. Other Observations

As described in Paper I, the galaxy and absorber sample is compiled from our own observations and from observations obtained from the literature. We summarize these observations in Table 3, which for each field lists the number of galaxies with spectroscopic redshifts available included into the analysis, the reference to the galaxy observations and analysis, the number of absorbers included into the analysis, and the reference to the absorber observations and analysis.

3. GALAXY IMAGE ANALYSIS

We analyzed all the galaxy images obtained with HST WFPC2 and determined various galaxy parameters following the procedures described in Paper I. We were able to determine a best-fit surface brightness profile for 142 galaxies, but not for 14 galaxies with disturbed morphologies, to which normal disk and bulge profiles cannot be applied. The results of the analysis are disk and bulge effective radii, disk-to-bulge ratio, orientation angle, disk inclination angle, bulge axis ratio, apparent magnitude and mean surface brightness (at the wavelength centroid of the filter response function) of the galaxies, rest-frame B -band absolute magnitude $M_B - 5 \log h$, morphological type (based on the diagnostics using the disk-to-bulge ratio), and rest-frame B -band mean surface brightness.

To determine the near-infrared luminosities of the galaxies, we applied standard galaxy photometry techniques. The apparent magnitude m_K was measured from the sum of the light within an isophot determined by the SExtractor program (Bertin & Arnouts 1996). Galaxy fluxes at near-infrared wavelengths were calibrated to the standard stars observed every night. A photometric solution was determined for each night using a linear function that consists of a zero point offset and an extinction coefficient as the two free parameters. The Vega magnitudes of the standard stars in K were converted to the AB magnitudes according to $AB(K) = K + 1.86$. Errors of the apparent magnitude measurements were determined from the corresponding 1σ error images by forming a quadratic sum of pixel values within the isophots. The rest-frame K -band absolute magnitude $M_K - 5 \log h$ was determined from the apparent magnitude m_K , corrected for the luminosity distance and the k correction. The rest-frame K -band luminosity of an L_* galaxy was taken to be $M_{K_*} = -21.6$ (Cowie et al. 1996).

To summarize, we present in Table 4 complete results of measurements for 157 galaxies in the 19 QSO fields. In columns (2)–(14) of Table 4, we list for each galaxy the field, Right Ascension and Declination offsets from the QSO $\Delta\alpha$ and $\Delta\delta$, redshift z_{gal} , impact parameter ρ , disk and bulge effective radii R_D and R_B , disk-to-bulge ratio D/B , orientation angle α , disk inclination angle i , bulge axis ratio b/a , apparent magnitude m_{WFPC2} (at the wavelength centroid of the filter response function), rest-frame B -band mean surface brightness $\langle\mu\rangle$, and absolute B -band magnitude $M_B - 5 \log h$. Measurement uncertainties in R_D and R_B were typically 2%, measurement uncertainties in D/B were typically 35%, measurement uncertainties in α and i were typically 2 deg, and measurement uncertainties in m_{WFPC2} and $M_B - 5 \log h$ were typically 0.2. In columns(15)–(16) of Table 4, we list respectively the apparent and absolute K -band magnitudes for 75 galaxies.

4. GALAXY AND ABSORBER PAIRS

The goal of the analysis is to investigate tenuous gas around galaxies. To accomplish the goal, it is necessary first to distinguish physical pairs from correlated and random pairs, which are formed either due to large-scale correlation between cluster galaxies and the galaxy that produces the absorber or by chance coincidence. We identify physical galaxy and absorber pairs according to the prescription described in Paper I. First, we accept absorption lines according to a 3σ detection threshold criterion, which is appropriate because the measurements are performed at a small number of known galaxy redshifts. Next, we adopt the cross-correlation function $\xi_{\text{ga}}(v, \rho)$ measured by Lanzetta, Webb, & Barcons (1997) and form galaxy and absorber pairs by requiring (1) $\xi_{\text{ga}} > 1$ (which excludes likely random pairs) and

(2) $\rho < 200 h^{-1}$ kpc (which from results of Lanzetta, Webb, & Barcons 1997 excludes likely correlated pairs). Next, we exclude galaxy and absorber pairs within 3000 km s^{-1} of the background QSOs (which are likely to be associated with the QSOs), and in three cases where more than one galaxy is paired with one absorber (absorber at $z_{\text{abs}} = 0.3786$ toward 0122–0021, absorber at $z_{\text{abs}} = 0.1670$ toward 0405–1219, and absorber at $z_{\text{abs}} = 0.4825$ toward 0454–2203) we choose the galaxy at the smallest impact parameter. Finally, we measure 3σ upper limits to absorption equivalent widths of galaxies that are not paired with corresponding absorbers, retaining only those measurements with 3σ upper limits satisfying $W < 0.35 \text{ \AA}$.

This procedure identifies 34 galaxy and Ly α absorber pairs and 13 galaxies that do not produce corresponding Ly α absorption lines to within sensitive upper limits. Redshifts of the galaxy and Ly α absorber pairs range from 0.0752 to 0.8920 with a median of 0.3567, and impact parameter separations of the galaxy and absorber pairs range from 12.4 to $175.2 h^{-1}$ kpc with a median of $62.2 h^{-1}$ kpc. The results are summarized in columns (17)–(18) of Table 4, which for each galaxy lists the absorber redshift z_{abs} , and the rest-frame equivalent width of the Ly α absorption line. Measurement uncertainties in W are typically 0.1 \AA . For completeness purpose, we also list in column (19) of Table 4 the results of the same analysis for the CIV absorption systems. The rest-frame CIV absorption equivalent width is measured for the line at $\lambda_{\text{rest}} = 1548 \text{ \AA}$.

In Table 4, galaxy entries without corresponding absorber entries represent cases for which the absorption measurement cannot be made, either because the galaxy occurs behind the QSO, the appropriate QSO spectrum is not available or lacks sensitivity, the spectral region containing the predicted Ly α or CIV line is blended with other absorption lines, or a corresponding Ly α or CIV absorption line was paired with a galaxy at a smaller impact parameter.

5. DESCRIPTIONS OF INDIVIDUAL FIELDS

Here we present brief descriptions of galaxies obtained from the new HST WFPC2 observations. We note galaxies by their coordinate offsets in Right Ascension and Declination, respectively, from the QSO line of sight in units of 0.1 arcsec. Individual galaxy images are shown in Figure 1. The spatial extent of each image is roughly $25 h^{-1}$ kpc on a side, and orientation of each image is arbitrary. Measurements for galaxies published previously in Paper I are listed in Table 4 together with the new ones.

5.1. The Field toward 0122–0021

Galaxy –00087–00123 at $z = 0.3788$ and $\rho = 47.1 h^{-1}$ kpc is a late-type spiral galaxy of luminosity $L_B = 0.69L_{B*}$ and color $M_B - M_K = 1.3$. This galaxy is associated with a corresponding Ly α absorption line with $W = 0.74 \text{ \AA}$ and a corresponding CIV absorption line with $W = 0.59 \text{ \AA}$ at $z = 0.3786$. The redshift determination of this galaxy is uncertain (Q=B in Lanzetta et al. 1995) and is therefore excluded from all analysis.

Galaxy –00168+00248 at $z = 0.3992$ and $\rho = 96.2 h^{-1}$ kpc is a late-type spiral galaxy of luminosity $L_B = 1.91L_{B*}$ and color $M_B - M_K = 1.8$. This galaxy is associated with a corresponding Ly α absorption line with $W = 2.38 \text{ \AA}$ and a corresponding CIV absorption line with $W = 1.70 \text{ \AA}$ at $z = 0.3989$.

Galaxy +00407–00092 at $z = 0.4299$ and $\rho = 138.9 h^{-1}$ kpc is a late-type spiral galaxy of luminosity $L_B = 0.30L_{B*}$ and color $M_B - M_K = 1.2$. This galaxy is associated with a corresponding Ly α absorption line at $z = 0.4302$ with $W = 0.84 \text{ \AA}$ and does not produce corresponding CIV absorption to within a sensitive upper limit. The redshift determination of this galaxy is uncertain (Q=B in Lanzetta et al. 1995) and is therefore excluded from all analysis.

Galaxy +00270–00372 at $z = 0.3793$ and $\rho = 143.9 h^{-1}$ kpc is a late-type spiral galaxy of luminosity $L_B = 0.76L_{B*}$ and color $M_B - M_K = 1.3$. This galaxy does not have a sensitive Ly α or CIV absorption measurement available.

5.2. The Field toward 0405–1219

We have published HST WFPC2 images of 14 galaxies surrounding the QSO in Paper I. Here we descriptions for two additional galaxies obtained from the new observations.

Galaxy +00073+00036 at $z = 0.5709$ and $\rho = 30.4 h^{-1}$ kpc is a late-type spiral galaxy of luminosity $L_B = 1.00L_{B*}$ and color $M_B - M_K = 1.3$. This galaxy (which occurs in the immediate vicinity of the QSO) does not produce corresponding Ly α or CIV absorption to within sensitive upper limits.

Galaxy –00014+00339 at $z = 0.1670$ and $\rho = 62.8 h^{-1}$ kpc shows a disturbed morphology, to which normal disk and bulge profiles cannot be applied. Assuming an irregular type galaxy spectral template, we estimate the K -band luminosity of the galaxy to be $L_K = 0.02L_{K*}$. This galaxy is associated with a corresponding Ly α absorption line with $W = 0.65 \text{ \AA}$ and a corresponding CIV absorption line with $W = 0.44 \text{ \AA}$ at $z = 0.1670$. This absorption system was studied previously by Spinrad et al. (1993). These authors attributed

this absorption system to a bright, early-type spiral galaxy +00405–00010 at $z = 0.1670$ and $\rho = 74.9 h^{-1}$ kpc, which fell out of the WFPC2 frame. We estimate the K -band luminosity of the galaxy to be $L_K = 1.20L_{K^*}$. It is likely that both galaxies contribute to the Ly α and CIV absorption lines (Chen & Prochaska 2000).

5.3. The Field toward 0903+1658

Galaxy +00066–00121 at $z = 0.4106$ and $\rho = 44.9 h^{-1}$ kpc is an early-type spiral galaxy of luminosity $L_B = 1.32L_{B^*}$ and color $M_B - M_K = 2.2$. Galaxy +00370+00251 at $z = 0.4100$ and $\rho = 145.5 h^{-1}$ kpc is an elliptical or S0 galaxy of luminosity $L_B = 0.63L_{B^*}$ and does not have a K -band luminosity measurement available. Galaxies –00398+00338 at $z = 0.4087$ and $\rho = 169.7 h^{-1}$ kpc and –00390+00358 at $z = 0.4094$ and $\rho = 172.2 h^{-1}$ kpc show signs of violent interaction, to which normal disk and bulge profiles cannot be applied. Galaxy –00379–00506 at $z = 0.4093$ and $\rho = 205.6 h^{-1}$ kpc is a late-type spiral galaxy of luminosity $L_B = 1.00L_{B^*}$ and color $M_B - M_K = 2.2$. Galaxy –00236+00663 at $z = 0.4115$ and $\rho = 229.4 h^{-1}$ kpc is a late-type spiral galaxy of luminosity $L_B = 0.58L_{B^*}$ and color $M_B - M_K = 1.0$. These galaxies (which occur in the immediate vicinity of the QSO) do not produce corresponding Ly α or CIV absorption to within sensitive upper limits.

Galaxy +00040–00171 at $z = 0.4258$ and $\rho = 58.2 h^{-1}$ kpc is a late-type spiral galaxy of luminosity $L_B = 0.30L_{B^*}$ and color $M_B - M_K = -0.3$. Galaxy –00032–00240 at $z = 0.5696$ and $\rho = 80.3 h^{-1}$ kpc shows a disturbed morphology, to which normal disk and bulge profiles cannot be applied. These two galaxies occur behind the QSO and so are excluded from all analysis.

Galaxies +00070+00350 at $z = 0.2690$ and $\rho = 91.8 h^{-1}$ kpc, –00361–00122 at $z = 0.2695$ and $\rho = 98.1 h^{-1}$ kpc, –00281+00513 at $z = 0.2697$ and $\rho = 150.7 h^{-1}$ kpc, and –00287+00536 at $z = 0.2702$ and $\rho = 156.8 h^{-1}$ kpc show disturbed morphologies, to which normal disk and bulge profiles cannot be applied. Galaxy –00178+00471 at $z = 0.2682$ and $\rho = 129.3 h^{-1}$ kpc is a late-type spiral galaxy of luminosity $L_B = 0.63L_{B^*}$ and color $M_B - M_K = 2.2$. These galaxies do not produce corresponding CIV absorption to within a sensitive upper limit, but do not have sensitive Ly α absorption measurements available.

5.4. The Field toward 1136–1334

Galaxy –00144–00095 at $z = 0.3191$ and $\rho = 49.2 h^{-1}$ kpc is an elliptical or S0 galaxy of luminosity $L_B = 0.58L_{B^*}$ and color $M_B - M_K = 1.6$. This galaxy does not produce

corresponding Ly α absorption to within a sensitive upper limit, but is associated with a corresponding CIV absorption line at $z = 0.3189$ with $W = 0.22 \text{ \AA}$.

Galaxy +00004+00233 at $z = 0.5550$ and $\rho = 86.3 h^{-1} \text{ kpc}$ shows a disturbed morphology, to which normal disk and bulge profiles cannot be applied. Galaxy +00442+00091 at $z = 0.5575$ and $\rho = 167.4 h^{-1} \text{ kpc}$ is an elliptical or S0 galaxy of luminosity $L_B = 0.33L_{B^*}$ and does not have a K -band luminosity measurement available. These two galaxies (which occurs in the immediate vicinity of the QSO) do not produce corresponding Ly α or CIV absorption to within sensitive upper limits.

Galaxy +00108–00255 at $z = 0.2044$ and $\rho = 59.4 h^{-1} \text{ kpc}$ is a late-type spiral galaxy of luminosities $L_B = 0.33L_{B^*}$ and color $M_B - M_K = 2.3$. This galaxy is associated with a corresponding CIV absorption line at $z = 0.2039$ with $W = 0.76 \text{ \AA}$, but does not have a sensitive Ly α absorption measurement available.

Galaxy –00271+00515 at $z = 0.3604$ and $\rho = 177.4 h^{-1} \text{ kpc}$ is a late-type spiral galaxy of luminosity $L_B = 0.28L_{B^*}$ and color $M_B - M_K = 2.0$. Galaxy –00073–00807 at $z = 0.3254$ and $\rho = 233.5 h^{-1} \text{ kpc}$ is a late-type spiral galaxy of luminosity $L_B = 1.45L_{B^*}$ and does not have a K -band luminosity measurement available. Galaxies –00365–00012 at $z = 0.2198$ and $\rho = 82.3 h^{-1} \text{ kpc}$, –00182–00483 at $z = 0.2123$ and $\rho = 113.6 h^{-1} \text{ kpc}$, and –00520+00138 at $z = 0.3598$ and $\rho = 163.8 h^{-1} \text{ kpc}$ are early-type spiral galaxies of luminosities between $L_B = 0.03L_{B^*}$ and $L_B = 2.29L_{B^*}$ and colors between $M_B - M_K = 2.1$ and $M_B - M_K = 2.2$. Galaxy –00451+00388 at $z = 0.3595$ and $\rho = 181.1 h^{-1} \text{ kpc}$ is an elliptical or S0 galaxy of luminosity $L_B = 1.58L_{B^*}$ and color $M_B - M_K = 2.9$. Galaxy –00032+00557 at $z = 0.1755$ and $\rho = 107.2 h^{-1} \text{ kpc}$ shows a disturbed morphology, to which normal disk and bulge profiles cannot be applied. These galaxies do not produce corresponding CIV absorption to within sensitive upper limits, but do not have sensitive Ly α absorption measurements available.

Galaxy +00019–00371 at $z = 0.6480$ and $\rho = 144.8 h^{-1} \text{ kpc}$ is an elliptical or S0 galaxy of luminosity $L_B = 1.45L_{B^*}$ and color $M_B - M_K = 1.8$. This galaxy occurs behind the QSO and so is excluded from all analysis.

Galaxy +00178–00542 at $z = 0.4007$ and $\rho = 183.6 h^{-1} \text{ kpc}$ is a late-type spiral galaxy of luminosity $L_B = 0.52L_{B^*}$ and color $M_B - M_K = 0.9$. This galaxy does not produce corresponding Ly α or CIV absorption to within a sensitive upper limit. The redshift determination of this galaxy is uncertain (Q=B in Lanzetta et al. 1995) and is therefore excluded from all analysis.

5.5. The Field toward 1216+0657

Galaxy +00372–00188 at $z = 0.1242$ and $\rho = 61.3 h^{-1}$ kpc is a late-type spiral galaxy of luminosity $L_B = 0.63L_{B*}$ and color $M_B - M_K = 1.2$. This galaxy is associated with a corresponding Ly α absorption line with $W = 1.26 \text{ \AA}$ and a corresponding CIV absorption line with $W = 0.31 \text{ \AA}$ at $z = 0.1243$.

Galaxy –00169–00569 at $z = 0.6021$ and $\rho = 226.1 h^{-1}$ kpc is a late-type spiral galaxy of luminosity $L_B = 1.58L_{B*}$ and color $M_B - M_K = 1.4$. Galaxy –00186–00893 at $z = 3.2720$ and $\rho = 320.4 h^{-1}$ kpc shows a compact morphology with a brightness profile best represented by the $R^{1/4}$ law and it is very bright. Therefore, it is likely to be a QSO. Galaxy +00496–00775 at $z = 0.4341$ and $\rho = 307.7 h^{-1}$ kpc is an early-type spiral galaxy of luminosity $L_B = 0.58L_{B*}$ and does not have a K -band luminosity measurement available. These objects occur behind the QSO and so are excluded from all analysis.

Galaxy –00606–00774 at $z = 0.0012$ and $\rho = 1.7 h^{-1}$ kpc is an elliptical or S0 galaxy of luminosity $L_B \ll 0.01L_{B*}$ and does not have a K -band luminosity measurement available. This galaxy does not have a sensitive Ly α or CIV absorption measurement available.

5.6. The Field toward 1259+5920

Galaxy +00270–00313 at $z = 0.1967$ and $\rho = 86.2 h^{-1}$ kpc is an elliptical or S0 galaxy of luminosity $L_B = 0.10L_{B*}$ and color $M_B - M_K = 1.6$. This galaxy is associated with a corresponding Ly α absorption line at $z = 0.1966$ with $W = 0.22 \text{ \AA}$, but does not produce corresponding CIV absorption to within a sensitive upper limit.

Galaxy –00605+00039 at $z = 0.5353$ and $\rho = 221.5 h^{-1}$ kpc is a late-type spiral galaxy of luminosity $L_B = 1.00L_{B*}$ and does not have a K -band luminosity measurement available. Galaxy +00087+00110 at $z = 0.4869$ and $\rho = 391.3 h^{-1}$ kpc is a late-type spiral galaxy of luminosity $L_B = 0.83L_{B*}$ and color $M_B - M_K = 1.5$. These two galaxies occur behind the QSO and so are excluded from all analysis.

Galaxy –00234+00685 at $z = 0.2412$ and $\rho = 173.6 h^{-1}$ kpc is a late-type spiral galaxy of luminosity $L_B = 0.48L_{B*}$ and color $M_B - M_K = 1.2$. This galaxy does not produce corresponding Ly α or CIV absorption to within a sensitive upper limit.

5.7. The Field toward 1317+2743

Galaxy +00068+00048 at $z = 0.6715$ and $\rho = 32.8 h^{-1}$ kpc is an elliptical or S0 galaxy of luminosity $L_B = 1.32L_{B^*}$ and does not have a K -band luminosity measurement available. This galaxy is associated with a corresponding Ly α absorption line at $z = 0.6716$ with $W = 0.78 \text{ \AA}$, but does not have a sensitive CIV absorption measurement available.

Galaxy –00444–00023 at $z = 0.6717$ and $\rho = 175.2 h^{-1}$ kpc is an elliptical or S0 galaxy of luminosity $L_B = 1.00L_{B^*}$ and does not have a K -band luminosity measurement available. This galaxy is associated with a corresponding Ly α absorption line at $z = 0.6736$ with $W = 0.78 \text{ \AA}$, but does not produce corresponding CIV absorption to within a sensitive upper limit.

Galaxies –00661+00105 at $z = 0.5397$ and $\rho = 245.3 h^{-1}$ kpc and –00681+00097 at $z = 0.5398$ and $\rho = 252.1 h^{-1}$ kpc show signs of violent interaction, to which normal disk and bulge profiles cannot be applied. These two galaxies do not produce corresponding Ly α absorption to within a sensitive upper limit, but do not have sensitive CIV absorption measurements available.

5.8. The Field toward 1424–1150

Galaxy +00030–00013 at $z = 0.8011$ and $\rho = 13.4 h^{-1}$ kpc is a late-type spiral galaxy of luminosity $L_B = 1.20L_{B^*}$ and does not have a K -band luminosity measurement available. This galaxy (which occur in the immediate vicinity of the QSO) does not produce corresponding Ly α or CIV absorption to within a sensitive upper limit.

Galaxy –00002+00176 at $z = 0.3404$ and $\rho = 52.0 h^{-1}$ kpc is a late-type spiral galaxy of luminosity $L_B = 0.63L_{B^*}$ and color $M_B - M_K = 2.0$. This galaxy is associated with a corresponding Ly α absorption line at $z = 0.3417$ with $W = 0.60 \text{ \AA}$, but does not produce corresponding CIV absorption to within a sensitive upper limit.

Galaxy –00114+00409 at $z = 0.1064$ and $\rho = 55.0 h^{-1}$ kpc is a late-type spiral galaxy of luminosity $L_B = 0.02L_{B^*}$ and does not have a K -band luminosity measurement available. Galaxy –00178+00864 at $z = 0.1038$ and $\rho = 111.9 h^{-1}$ kpc is an elliptical or S0 galaxy of luminosity $L_B = 0.13L_{B^*}$ and color $M_B - M_K = 2.3$. Galaxies –00881–00478 at $z = 0.1045$ and $\rho = 127.9 h^{-1}$ kpc and –00913–00538 at $z = 0.2597$ and $\rho = 266.6 h^{-1}$ kpc are early-type spiral galaxies of luminosities $L_B = 0.13L_{B^*}$ and $L_B = 0.36L_{B^*}$, respectively, and do not have K -band luminosity measurements available. These galaxies do not have sensitive Ly α or CIV absorption measurements available.

Galaxy –00691–00339 at $z = 0.3942$ and $\rho = 245.7 h^{-1}$ kpc is a late-type spiral galaxy of luminosity $L_B = 0.25L_{B*}$ and does not have a K -band luminosity measurement available. This galaxy does not produce corresponding Ly α or CIV absorption to within a sensitive upper limit.

5.9. The Field toward 1641+3954

Galaxies +00068–00013 at $z = 0.5880$ and $\rho = 26.2 h^{-1}$ kpc, –00108+00279 at $z = 0.5900$ and $\rho = 113.2 h^{-1}$ kpc, –00366+00366 at $z = 0.5934$ and $\rho = 196.2 h^{-1}$ kpc, and –00621+00065 at $z = 0.5917$ and $\rho = 236.5 h^{-1}$ kpc are late-type spiral galaxies of luminosities in the range $L_B = 1.00L_{B*}$ to $1.10L_{B*}$. Galaxies +00289–00369 at $z = 0.5918$ and $\rho = 177.5 h^{-1}$ kpc is an elliptical or S0 galaxies of luminosity $L_B = 1.45L_{B*}$. These galaxies (which occur in the immediate vicinity of the QSO) do not produce corresponding Ly α or CIV absorption to within a sensitive upper limit.

Galaxies +00122–00189 at $z = 0.2813$ and $\rho = 59.5 h^{-1}$ kpc, –00208+00107 at $z = 0.4126$ and $\rho = 76.4 h^{-1}$ kpc, +00322+00625 at $z = 0.2410$ and $\rho = 168.5 h^{-1}$ kpc, and +00256–00668 at $z = 0.2192$ and $\rho = 160.9 h^{-1}$ kpc are late-type spiral galaxies of luminosities between $L_B = 0.04L_{B*}$ and $0.36L_{B*}$. Galaxies +00406–00388 at $z = 0.3316$ and $\rho = 163.6 h^{-1}$ kpc, and –00506–00327 at $z = 0.4055$ and $\rho = 195.0 h^{-1}$ kpc are elliptical or S0 galaxies of luminosities $L_B = 0.40L_{B*}$. These galaxies do not have sensitive Ly α or CIV absorption measurements available.

Galaxy –00164–00157 at $z = 0.5319$ and $\rho = 82.7 h^{-1}$ kpc is a late-type spiral galaxy of luminosity $L_B = 0.76L_{B*}$. This galaxy is associated with a corresponding Ly α absorption line at $z = 0.5342$ with $W = 1.11 \text{ \AA}$, but does not have a sensitive CIV absorption measurement available.

Galaxy –00441+00323 at $z = 0.6944$ and $\rho = 217.4 h^{-1}$ kpc is a late-type spiral galaxy of luminosity $L_B = 2.09L_{B*}$. This galaxy occurs behind the QSO and so is excluded from all analysis.

Galaxies –00183+00646 at $z = 0.5296$ and $\rho = 244.3 h^{-1}$ kpc and +00321–00834 at $z = 0.5289$ and $\rho = 325.0 h^{-1}$ kpc are elliptical or S0 galaxies of luminosities $L_B = 0.83L_{B*}$ and $L_B = 1.20L_{B*}$, respectively. These two galaxies do not produce corresponding Ly α absorption to within a sensitive upper limit, but do not have sensitive CIV absorption measurements available.

We do not have K -band photometry for this field.

5.10. The Field toward 2251+1552

Galaxy +00322–00003 at $z = 0.3529$ and $\rho = 97.0 h^{-1}$ kpc is a late-type spiral galaxy of luminosity $L_B = 0.63L_{B*}$ and color $M_B - M_K = 1.3$. This galaxy is associated with a corresponding Ly α absorption line at $z = 0.3526$ with $W = 0.70 \text{ \AA}$, but does not produce corresponding CIV absorption to within a sensitive upper limit.

6. ANALYSIS

In order to determine how the extent of tenuous gas around galaxies depends on galaxy properties, we performed in Paper I a maximum likelihood analysis to (1) confirm the existence of a fiducial relationship between some measure of the strength of neutral hydrogen absorption (e.g. Ly α absorption equivalent width W or neutral hydrogen column density N) and galaxy impact parameter and (2) assess whether accounting for measurements of other galaxy properties (such as galaxy B -band luminosity L_B , effective radius r_e , mean surface brightness $\langle\mu\rangle$, disk-to-bulge ratio D/B , or redshift z) can improve upon the fiducial relationship. Here we examine whether or not the results of previous analysis can be retained and improved by including additional measurements. First, we consider two different geometries of gas distribution—a spherical halo model and a flattened disk model—and repeat the maximum-likelihood analysis based on the new larger galaxy and absorber pair sample to determine the best-fit model and the intrinsic variation, σ_c . Next, we determine whether accounting for galaxy near-infrared photometry can improve the fiducial relationship between Ly α absorption equivalent width and galaxy impact parameter. Finally, we continue to examine the HST WFPC2 images of the additional galaxies to determine whether extended gas arises as a result of galaxy interactions, as evidenced by disturbed morphologies or the presence of close companions.

6.1. The Relation between Galaxies and Ly α Absorption Systems

To confirm the existence of a fiducial relationship between some measure of the strength of neutral hydrogen absorption (e.g. Ly α absorption equivalent width W or neutral hydrogen column density N) and galaxy impact parameter ρ , we adopt the parameterized linear form

$$y = a_1x_1 + \text{constant.} \tag{1}$$

The “dependent measurement” y represents the strength of neutral hydrogen absorption and may be $\log W$, $\log (W \cos i)$, $\log N$, or $\log (N \cos i)$. (The $\cos i$ factor is included as a

path-length correction in models of inclined galaxy disks.) The “independent measurement” x_1 represents some measure of the distance between the absorber and the galaxy and may be $\log \rho$ for a spherical halo model or $\log R$ for a flattened disk model. Here the galactocentric radius R is related to the galaxy impact parameter ρ by

$$R = \rho \left[1 + \sin^2 \alpha \tan^2 i \right]^{1/2}, \quad (2)$$

where α is the orientation angle between the apparent major axis of the galaxy and the projected line segment joining the galaxy to the QSO.

To assess whether accounting for measurements of other galaxy properties (in addition to galaxy impact parameter) can improve upon the fiducial relationship, we adopt the parameterized bi-linear form

$$y = a_1 x_1 + a_2 x_2 + \text{constant}. \quad (3)$$

The additional “independent measurement” x_2 represents galaxy properties and may be $\log L_B$, $\log r_e$, $\langle \mu \rangle$, $\log D/B$, or $\log(1+z)$. The goodness of fit for each model is estimated based on a “confidence interval test” and an “anti-correlation test”. Results of the statistical tests of each model is presented in Table 5, which lists the measurements; the statistical significances $a/\delta a$ of the fitting coefficients; the correlation coefficients r_{gk} , r_k , r_s , and r_p and the corresponding statistical significances r_{gk}/σ_{gk} , r_k/σ_k , r_s/σ_s , and r_p/σ_p of the generalized Kendall, Kendall, Spearman, and Pearson correlation tests, respectively; and the cosmic scatter σ_c .

Comparison of the results in Table 5 and the ones presented in Paper I shows that (1) the anti-correlation between Ly α absorption equivalent width and galaxy impact parameter remains at a higher significance level, (2) including galaxy B -band luminosity, effective radius, or redshift as an additional scaling factor continues to substantially improve the W versus ρ anti-correlation, and (3) including galaxy mean surface brightness or disk-to-bulge ratio as an additional scaling factor remains statistically identical to the fiducial relationship between W and ρ . The similarity between the results accounting for galaxy B -band luminosity and the ones accounting for galaxy effective radius may be attributed to the Holmberg (1975) relation between galaxy luminosity and size, and the similarity between the results accounting for galaxy B -band luminosity and the ones accounting for galaxy redshift to the selection effect due to a magnitude-limited survey. The latter is demonstrated in Figure 1 of Chen, Lanzetta, & Fernández-Soto (2000), which shows the residuals of the W vs. ρ anti-correlation after accounting for galaxy B -band luminosity as a function of galaxy redshift. No correlation is found between the residuals and galaxy redshifts. Therefore, we confirm that the amount of gas intercepted along the line of sight depends on galaxy impact

parameter and B -band luminosity, but does not depend strongly on galaxy mean surface brightness, disk-to-bulge ratio, or redshift.

To illustrate the dependence/independence of $\text{Ly}\alpha$ absorption equivalent width on various galaxy parameters, we plot in Figure 1 the residuals of the W versus ρ anti-correlation as a function of galaxy B -band luminosity (the upper-left panel), redshift (the upper-right panel), galaxy mean surface brightness (the lower-left panel), and galaxy disk-to-bulge ratio (the lower-right panel). Circles represent elliptical or S0 galaxies; triangles represent early-type spiral galaxies; and squares represent late-type spiral galaxies. Points with arrows indicate 3σ upper limits. The residuals appear to correlate strongly only with galaxy B -band luminosity, but not with galaxy redshift, mean surface brightness, or disk-to-bulge ratio. Note that Figure 1 also indicates the survey range of the galaxy and absorber pair sample in various galaxy parameter spaces. Specifically, of all the 47 galaxies in the sample, two are of luminosities $L_B < 0.04L_{B*}$ at redshifts $z = 0.0949$ and $z = 0.1380$, respectively, and 13 are of luminosities $0.04 L_{B*} \lesssim L_B \lesssim 0.25 L_{B*}$ with redshifts spanning from $z = 0.0915$ to $z = 0.6350$. Namely, 32% of the sample is made up of faint dwarf galaxies that span a wide redshift range. Furthermore, the dotted line in the lower-left panel divides between low surface brightness galaxies and high surface brightness ones.⁴ Therefore, six of the 47 galaxies (13%) are low surface brightness galaxies at redshifts between $z = 0.0915$ to $z = 0.3180$. Finally, the lower-right panel indicates that galaxies in the sample span a wide range in the disk-to-bulge ratio, from bulge-dominated galaxies to disk-dominated galaxies.

To study whether tenuous gas is distributed around galaxies in flattened disks, in which case the absorption signatures should occur preferentially in galaxies of low inclination angles, or in spherical halos, in which case the absorption signatures should be independent of galaxy inclination and orientation, we compare the statistical significances of the W versus ρ and W versus R anti-correlations. In Paper I, we were unable to distinguish between a spherical halo model and a flattened disk model because of the statistically identical results of the tests. The results presented in Table 5 based on the larger galaxy and absorber sample, however, indicate that although the strong anti-correlations between W and R remain (rows 7 to 13), they are now marginally inferior to the W versus ρ anti-correlations (rows 1 to 6). Specifically, the anti-correlation test indicates that the anti-correlation between W and ρ is at a level of significance ranging from 4.1σ to 5.3σ , while the anti-correlations between $W \cos i$ and R is at a level of significance ranging from 3.2σ to 4.0σ ; the anti-correlation between W , ρ , and L_B is at a level of significance ranging from 5.2σ to 7.1σ , while the

⁴The value is determined by adopting a B -band central surface brightness, $\mu_0 = 23.0 \text{ mag sec}^{-2}$ and transforming to the corresponding mean surface brightness within the Holmberg radius, assuming an exponential disk profile.

anti-correlations between $W \cos i$, R , and L_B is at a level of significance ranging from 4.7σ to 6.2σ . Given that several highly inclined disk galaxies with a 90-degree orientation angle to the QSOs are directly observed in our sample (e.g. galaxy +00106+00057 toward 0454–2203 and galaxy –00042–00038 toward 1622+2352), we attribute the W versus R anti-correlation to the correlation between ρ and R defined in Equation (2) and conclude that tenuous gas is more likely to be distributed in a spherical halo than in a flattened disk.

To summarize, the results of the likelihood analysis show that tenuous gas around galaxies may be described by

$$\log W = -(0.96 \pm 0.11) \log \rho + \text{constant}, \quad (4)$$

and is better described by

$$\log W = -\alpha \log \rho + \beta \log L_B + \text{constant}, \quad (5)$$

where

$$\alpha = 1.04 \pm 0.10 \quad (6)$$

and

$$\beta = 0.40 \pm 0.09. \quad (7)$$

Roughly relating Ly α absorption equivalent width W to neutral hydrogen column density N according to the prescription described by Lanzetta et al. (1995) and in Paper I, tenuous gas around galaxies may also be described by

$$\log \left(\frac{N}{10^{20} \text{ cm}^{-2}} \right) = -\alpha \log \left(\frac{\rho}{10 \text{ kpc}} \right) + \beta \log \left(\frac{L_B}{L_{B*}} \right) + \text{constant} \quad (8)$$

where

$$\alpha = 5.56 \pm 0.42, \quad (9)$$

$$\beta = 2.56 \pm 0.43, \quad (10)$$

and

$$\text{constant} = 1.56 \pm 0.78. \quad (11)$$

Comparisons of the data and the best-fit models are presented in Figures 3, 4 and 5 with the estimated cosmic scatter of each relationship shown in the upper-right corner.

6.2. Gaseous Extent as a Function of Galaxy K -Band Luminosity

We have confirmed in §§ 6.1 that the extent of tenuous gas around galaxies scales with galaxy B -band luminosity. Interpreting this scaling relation is difficult, because B -band

luminosity is sensitive to recent star formation activity, which is expected to be stronger in galaxies of later types, but our analysis also indicates that the extent of tenuous gas around galaxies is insensitive to galaxy morphology. It appears that galaxy B -band luminosity may not be a true fundamental parameter. Because K -band luminosity is sensitive to the old stellar content and is considered to be a good measure of the total stellar mass (Bruzual & Charlot 1993), here we consider the possibility that the amount of gas intercepted along the line of sight depends on galaxy rest-frame K -band luminosity L_K .

Considering only galaxies with K -band photometric measurements available leaves 20 galaxy and absorber pairs and two galaxies that do not produce corresponding $\text{Ly}\alpha$ absorption lines to within sensitive upper limits. Adopting a power-law relationship between W and ρ and L_K , we find according to the likelihood analysis that tenuous gas around galaxies may be described by

$$\log W = -\alpha \log \rho + \beta_k \log L_K + \text{constant} \quad (12)$$

where

$$\alpha = 1.25 \pm 0.18 \quad (13)$$

and

$$\beta_k = 0.35 \pm 0.08. \quad (14)$$

The result applies over the K -band luminosity interval $0.005 L_{K*} \lesssim L_K \lesssim 3.3 L_{K*}$ spanned by the observations. Comparison of the data and the best-fit model is shown in the left panel of Figure 6.

For comparison, we repeat the likelihood analysis for the subsample, but replacing galaxy K -band luminosity with galaxy B -band luminosity. Results of the analysis yield $\alpha = 1.16 \pm 0.17$ and $\beta = 0.50 \pm 0.11$. The result applies over the B -band luminosity interval $0.04 L_{B*} \lesssim L_B \lesssim 2.6 L_{B*}$ spanned by the subsample. Comparison of the data and the best-fit model is shown in the right panel of Figure 6. The results of the statistical tests for the subsample are presented in Table 6.

We find that the W versus ρ anti-correlation accounting for galaxy K -band luminosity and the one accounting for galaxy B -band luminosity are both superior to the fiducial W versus ρ anti-correlation, indicating that the extent of tenuous gas around galaxies depends sensitively on galaxy K -band luminosity. In addition, although the results of the statistical tests indicate that the W versus ρ anti-correlation accounting for L_B is statistically comparable to the W versus ρ anti-correlation accounting for L_K , the cosmic scatter σ_c in the latter case is further reduced by a substantial amount (33%). Because of the marginally stronger scaling relation between the gaseous extent of galaxies and galaxy K -band luminosity and because galaxies of all morphological types possess extended gaseous halos, we find that

galaxy mass is likely to be the dominant factor that determines the extent of tenuous gas around galaxies. The similarity between the results accounting for galaxy B -band luminosity and the ones accounting for galaxy K -band luminosity may be attributed to the strong correlation between galaxy K -band and B -band luminosities for galaxies in the sample as shown in Figure 7.

6.3. Galaxy Interactions

By carefully examining HST WFPC2 images of galaxies in our sample, we found in Paper I no evidence that galaxy interactions play an important role in distributing tenuous gas around galaxies in all cases. Here we investigate whether this result remains valid for the additional galaxies in the new nine QSO fields. We examine whether or not galaxies in the new sample exhibit close companions or disturbed morphologies in the HST WFPC2 images. Of all the galaxies presented in Figure 1, only galaxy $-00014+00339$ toward $0405-1219$ appears to exhibit obvious signs of a disturbed morphology and is associated with a corresponding Ly α absorption line at $z = 0.167$. (But galaxy $+00405-00010$ toward $0405-1219$ also occurs at the same redshift and is likely to contribute to the Ly α absorption system.) Galaxy $-00032+00557$ toward $1136-1334$ and galaxies $+00070+00350$, $-00361-00122$, $-00281+00513$, and $-00287+00536$ toward $0903+1658$, which occur at small impact parameters (between $\rho = 80.3 h^{-1}$ kpc and $\rho = 156.8 h^{-1}$ kpc), appear to have disturbed morphologies but do not have sensitive Ly α absorption measurements available. Galaxy $+00004+00233$ toward $1136-1334$, and galaxies $-00398+00338$ and $-00390+00358$ toward $0903+1658$, which occur in the immediate vicinity of the QSOs, appear to have disturbed morphologies and do not produce corresponding Ly α absorption lines to within a sensitive upper limit. The galaxy pair $-00661+00105$ and $-00681+00097$ at $z \approx 0.5398$ toward $1317+2743$, which occurs at relatively large impact parameters ($\rho \approx 250 h^{-1}$ kpc), appears to have disturbed morphologies and does not produce a corresponding Ly α absorption line to within a sensitive upper limit. Based on the new galaxy sample, we confirm that there is no evidence that tenuous gas is distributed around galaxies as a result of galaxy interactions in most cases, although we cannot rule out the possibility that tenuous gas is distributed around galaxies as a result of galaxy interactions in some cases.

Additional support may be inferred based on the results shown in the lower-right panel of Figure 2 that the residuals of the W vs. ρ relationship do not correlate strongly with galaxy morphology as represented by the disk-to-bulge ratio. Given the apparent morphology-density relation observed for galaxies in the local universe (e.g. Dressler et al. 1997), we find it unlikely that gaseous extent of galaxies is correlated with the surrounding galaxy

environment.

7. DISCUSSION

Adopting a quantitative criterion to identify physical galaxy and absorber pairs, we have repeated the likelihood analysis to study the relation between Ly α absorption systems and galaxies. Considering only galaxy and absorber pairs that are likely to be physically associated and excluding galaxy and absorber pairs within 3000 km s $^{-1}$ of the background QSOs leaves 34 galaxy and absorber pairs and 13 galaxies that do not produce corresponding Ly α absorption lines to within sensitive upper limits. We confirm that the amount of gas encountered along the line of sight depends on the galaxy impact parameter ρ and galaxy B -band luminosity L_B but does not depend strongly on the galaxy mean surface brightness $\langle\mu\rangle$, disk-to-bulge ratio D/B , or redshift z and that there is no evidence that galaxy interactions play an important role in distributing tenuous gas around galaxies in most cases. We also demonstrate that the amount of gas encountered along the line of sight also depends on galaxy K -band luminosity L_K and that tenuous gas is likely to be distributed in spherical halos, rather than in flattened disks.

The statistically significant anti-correlation between Ly α absorption equivalent width and galaxy impact parameter strongly supports that most absorbers are indeed associated with the individual galaxies identified. Most importantly, we show that extended gaseous halos are a common and generic feature of galaxies of all morphological types and that galaxy mass is the dominant factor that determines the extent of tenuous gas around galaxies. The strong scaling relationship between Ly α absorption equivalent width and galaxy luminosity further supports that the absorbers trace tenuous gas in individual halos surrounding the galaxies rather than tenuous gas in galaxy groups or large-scale filaments around the galaxies. Although we cannot exclude the possibility that the absorbers may arise in a population of dwarfs bound in a larger potential well, the scaling relationship strongly argues that the absorption gas cross section is determined by the luminous galaxies identified in our survey. In addition, Bothun et al. (1993) have shown that low surface brightness disk galaxies (with scale size between 1 and 5 kpc) tend to avoid virialized regions and are less clustered. It would be therefore very uncharacteristic to find low surface brightness galaxies in addition to the galaxies identified in our survey within a radius of 200 kpc from the sightline and ± 250 km s $^{-1}$ away from the absorber redshifts. Here we discuss the implications drawn from the results of our analysis.

7.1. The Incidence and Extent of Tenuous Gas Around Galaxies

Adopting the results of the likelihood analysis presented in §§ 6.1, we update the scaling relationship between the gaseous extent r of galaxies and galaxy B -band luminosity L_B . We find in a complete agreement with our previous analysis that the extent of tenuous gas around galaxies scales with galaxy B -band luminosity by

$$\frac{r}{r_*} = \left(\frac{L_B}{L_{B*}} \right)^{t_B}, \quad (15)$$

where $t_B = \beta/\alpha$ and is estimated based on Equations (6) and (7) to be

$$t_B = 0.39 \pm 0.09, \quad (16)$$

and that the gaseous extent of a typical L_* galaxy is

$$r_* = 184^{+29}_{-25} h^{-1} \text{ kpc} \quad (17)$$

at a Ly α absorption equivalent width threshold $W = 0.3 \text{ \AA}$. The results apply over the B -band luminosity interval $0.03 \lesssim L_B \lesssim 2.6L_{B*}$ and for galaxies of all morphological types spanned by the observations.

Adopting the results of the likelihood analysis presented in §§ 6.2, we also determine the scaling relationship between the gaseous extent of galaxies and galaxy K -band luminosity L_K . We find that the extent of tenuous gas around galaxies scales with galaxy K -band luminosity by

$$\frac{r}{r_*} = \left(\frac{L_K}{L_{K*}} \right)^{t_K}, \quad (18)$$

where

$$t_K = 0.28 \pm 0.08 \quad (19)$$

and

$$r_* = 177^{+30}_{-26} h^{-1} \text{ kpc} \quad (20)$$

based on Equations (13) and (14) at a Ly α absorption equivalent width threshold $W = 0.3 \text{ \AA}$. The results apply over the K -band luminosity interval $0.005 \lesssim L_K \lesssim 3.3L_{K*}$ and for galaxies of all morphological types spanned by the observations.

To estimate the incidence and covering factor of tenuous gas in the extended halos, we perform a maximum-likelihood analysis with the probability that a galaxy gives rise to an absorption system of some absorption equivalent width threshold written as

$$P = \epsilon H[r(L_B) - \rho] \kappa(\rho), \quad (21)$$

where ϵ is the fraction of galaxies that give rise to Ly α absorption, H is the Heaviside step function that accounts for the scaling relationship between the gaseous extent of galaxies and galaxy B -band luminosity, and κ is the covering factor of tenuous gas in the extended halos. The likelihood of detecting an ensemble of galaxies, n of which give rise to Ly α absorption systems and m of which do not, is given by

$$\mathcal{L} = \prod_{i=1}^n \epsilon H[r(L_{B_i}) - \rho_i] \kappa(\rho_i) \times \prod_{j=1}^m \{1 - \epsilon H[r(L_{B_j}) - \rho_j] \kappa(\rho_j)\}. \quad (22)$$

Because it is difficult to separate ϵ from κ , we choose to simply determine the mean value of the product $\langle \epsilon \kappa \rangle$ as a result. The likelihood function may therefore be written as

$$\mathcal{L} = \prod_{i=1}^n \langle \epsilon \kappa \rangle \prod_{j=1}^m (1 - \langle \epsilon \kappa \rangle) \quad (23)$$

$$= \langle \epsilon \kappa \rangle^n (1 - \langle \epsilon \kappa \rangle)^m. \quad (24)$$

Based on the scaled W versus ρ anti-correlation presented in Figure 4, we find that only two of the 31 galaxies at impact parameter $\rho < 180 h^{-1}$ kpc do not produce corresponding Ly α absorption lines to within sensitive upper limits, while 11 of the 16 galaxies at impact parameter $\rho > 180 h^{-1}$ kpc do not produce corresponding Ly α absorption lines to within sensitive upper limits. The maximum likelihood analysis yields a best estimate of $\langle \epsilon \kappa \rangle = 0.94$ with a 1σ lower bound of $\langle \epsilon \kappa \rangle = 0.86$ for tenuous gas within a radius of 180 kpc around the galaxies.

We conclude that, at the rest-frame absorption equivalent width threshold $W \gtrsim 0.3 \text{ \AA}$ (corresponding to a neutral hydrogen column density threshold $N(\text{HI}) \gtrsim 1.3 \times 10^{14} \text{ cm}^{-2}$), most galaxies are surrounded by extended gaseous halos of $\approx 180 h^{-1}$ kpc radius with a covering factor of 94%. The agreement between Equations (17) and (20) demonstrates that the ground-based near-infrared photometry agrees very well with the space-based optical photometry and further supports that a typical L_* galaxy, independent of morphological type, does indeed possess an extended gaseous halo of radius $\approx 180 h^{-1}$ kpc.

7.2. Implications for The Evolution of Star Formation Rate Density

The scaling relationship between the extent of tenuous gas around galaxies and galaxy luminosity provides a means of quantitatively relating statistical properties of Ly α absorption systems to statistical properties of faint galaxies. We have pointed out in Paper I that given a known galaxy population and the known scaling relation we can estimate the fraction of Ly α absorption systems that originate in extended gaseous halos of galaxies. But we have

also demonstrated that the prediction may vary from 30% to 100%. The large uncertainty is primarily due to the uncertainties in the normalization and the faint-end slope of the galaxy luminosity function. The result also reflects the generic difficulty in understanding galaxy formation and evolution based on comparisons of observational quantities obtained from magnitude-limited galaxy surveys (which suffer from various selection biases) and theoretical predictions.

As discussed by Chen, Lanzetta, & Fernández-Soto (2000), the predicted number density of Ly α absorption systems arising in the extended gaseous halos of galaxies may be given by

$$n(z) = \frac{c}{H_0}(1+z)(1+2q_0z)^{-1/2} \int_0^\infty d\left(\frac{L_B}{L_{B*}}\right) \Phi(L_B, z)\sigma(L_B)\kappa\epsilon, \quad (25)$$

where c is the speed of light, $\Phi(L_B, z)$ is the galaxy luminosity function, σ is the H I absorbing gas cross section that scales with galaxy B -band luminosity, κ is the halo covering factor, and ϵ is the fraction of galaxies that produce corresponding Ly α absorption systems. Substituting the scaling relationship according to Equations (15), (16), and (17), and adopting the result of §§ 7.1 that most galaxies are surrounded by extended gaseous halos of $\approx 180 h^{-1}$ kpc radius with a roughly unity covering factor, we find

$$n(z) = \frac{c}{H_0}(1+z)(1+2q_0z)^{-1/2} \int_0^\infty d\left(\frac{L_B}{L_{B*}}\right) \left(\frac{L_B}{L_{B*}}\right)^{0.8} \Phi(L_B, z)\pi r_*^2. \quad (26)$$

For comparison, the comoving B -band luminosity density is defined as

$$\mathcal{L}_B(z) = \int_0^\infty d\left(\frac{L_B}{L_{B*}}\right) L_B \Phi(L_B, z). \quad (27)$$

We can therefore relate the predicted number density of Ly α absorption systems with $\mathcal{L}_B(z)$ by

$$n(z) = \frac{c}{H_0}(1+z)(1+2q_0z)^{-1/2} \left(\frac{\pi r_*^2}{L_{B*}}\right) \mathcal{L}_B(z) \mathcal{O}(L_B), \quad (28)$$

where $\mathcal{O}(L_B)$ accounts for the departure of the mean absorption gas cross section averaged over galaxies of different luminosities per unit comoving volume from the comoving B -band luminosity density and is defined as

$$\mathcal{O}(L_B) = \int_0^\infty d\left(\frac{L_B}{L_{B*}}\right) \left(\frac{L_B}{L_{B*}}\right)^{0.8} \Phi(L_B, z) / \int_0^\infty d\left(\frac{L_B}{L_{B*}}\right) \left(\frac{L_B}{L_{B*}}\right) \Phi(L_B, z). \quad (29)$$

Performing these integrals, we find

$$\mathcal{O}(L_B) = \Gamma(1.8)/\Gamma(2.0) = 0.93 \sim 1.0, \quad (30)$$

where Γ is the gamma function.

It appears that the number density evolution of Ly α absorption systems traces the evolution of the comoving galaxy B -band luminosity density. Although the results of the analysis presented in §§ 6.2 indicate that galaxy mass (as probed by galaxy K -band luminosity), rather than recent star formation activity (as probed by galaxy B -band luminosity) is the dominant factor that determines the gaseous extent around galaxies, we argue that Equation (28) is valid so long as the strong correlation between galaxy K -band and B -band luminosities seen in our survey (Figure 7) remains for galaxies at higher redshifts.

Comparing the measurements of the Ly α absorption line density obtained by Weymann et al. (1998) at redshifts $z < 1.5$ with the ones obtained by Bechtold (1994) at redshifts $z > 1.5$ (see Chen et al. 2000), we find that the number density of Ly α absorption systems increases gradually with redshift, implying a steadily increasing comoving B -band luminosity density over the entire redshift range ($0 \lesssim z \lesssim 4$). The predicted shallow slope of the comoving B -band luminosity density as a function of redshift at redshifts $z < 1$ (where the scaling relation between the gaseous extent of galaxies and galaxy B -band luminosity is well understood and measured) agrees better with the results presented by Cowie, Songaila, & Barger (1999), but disagrees with the steep slope presented by Lilly et al. (1996). On the other hand, it is in a broad agreement with recent measurements of luminosity density evolution at higher redshifts (Pascarella et al. 1998; Steidel et al. 1999). Namely, the comoving galaxy luminosity density does not fall off at redshifts beyond $z = 3$.

An accurate assessment of luminosity density evolution bears importantly on discriminating between different galaxy formation scenarios (e.g. Somerville & Primack 1998). A flat or steadily increasing galaxy luminosity density would imply that the bulk of star formation occurs much earlier (c.f. Madau, Pozzetti, & Dickinson 1998), which would present a serious challenge to the hierarchical formation model. We have demonstrated that if (1) all the observed Ly α absorption systems of neutral hydrogen column density $N(\text{HI}) \gtrsim 10^{14} \text{ cm}^{-2}$ arise in extended gaseous halos around galaxies and (2) the scaling relation applies to absorbers at all redshifts, then the number density evolution of Ly α absorption systems may serve to constrain the measurements of cosmic star formation rate density.

8. SUMMARY AND CONCLUSIONS

We present complete results of a program to obtain and analyze HST WFPC2 images and ground-based K' images of galaxies identified in an imaging and spectroscopic survey of faint galaxies in fields of HST spectroscopic target QSOs. We measure properties of 142

galaxies, of which 40 are associated with corresponding Ly α absorption systems and 47 do not produce corresponding Ly α absorption lines to within sensitive upper limits. The galaxy and absorber pair sample is about 50% larger than the one previously published in Paper I. We repeat the likelihood analysis to examine whether or not the results of previous analysis may be retained and further improved by including additional measurements.

Following Paper I, we consider galaxy and absorber pairs physically correlated if (1) the galaxy–absorber cross-correlation amplitude satisfies $\xi_{\text{ga}}(v, \rho) > 1$ and (2) the galaxy impact parameter satisfies $\rho < 200 h^{-1}$ kpc. Including only galaxy and absorber pairs that are likely to be physically associated and excluding galaxy and absorber pairs within 3000 km s $^{-1}$ of the background QSOs leaves 34 galaxy and absorber pairs and 13 galaxies that do not produce corresponding Ly α absorption lines to within sensitive upper limits. Redshifts of the galaxy and absorber pairs range from $z = 0.0752$ to 0.8920 with a median of $z = 0.3567$, and impact parameter separations of the galaxy and absorber pairs range from $\rho = 12.4$ to 175.2 h^{-1} kpc with a median of $\rho = 62.2 h^{-1}$ kpc. Of the 47 galaxies, 15 (32%) are of B -band luminosity $L_B < 0.25 L_{B^*}$ with redshifts ranging from $z = 0.0915$ to $z = 0.6350$, and six (13%) are of low surface brightness with redshifts ranging from $z = 0.0915$ to $z = 0.3180$.

We confirm the results previously published in Paper I with improved statistics that the amount of gas encountered along the line of sight depends on the galaxy impact parameter ρ , galaxy B -band luminosity L_B , but does not depend strongly on the galaxy mean surface brightness $\langle \mu \rangle$, disk-to-bulge ratio D/B , or redshift z and that there is no evidence that galaxy interactions play an important role in distributing tenuous gas around galaxies in most cases. Furthermore, we find that:

1. The anti-correlation between Ly α absorption equivalent width W and galaxy impact parameter ρ accounting for galaxy K -band luminosity L_K is superior to the fiducial relationship between W and ρ . We conclude that the amount of gas intercepted along the line of sight depends on galaxy K -band luminosity which, together with the fact that galaxies of all morphological types possess extended gaseous halos, indicates that galaxy mass is likely to be the dominant factor that determines the extent of tenuous gas around galaxies.

2. The relationship between galaxy gaseous radius r and galaxy K -band luminosity L_K may be described by

$$\frac{r}{r_*} = \left(\frac{L_K}{L_{K^*}} \right)^{t_K}, \quad (31)$$

with

$$t_K = 0.28 \pm 0.08 \quad (32)$$

and

$$r_* = 177_{-26}^{+30} h^{-1} \text{ kpc} \quad (33)$$

for a Ly α absorption equivalent width threshold $W = 0.3 \text{ \AA}$. The $t = 0$ case (no dependence of gaseous radius on galaxy K -band luminosity) can be ruled out at the 3.5σ level of significance.

3. At the rest-frame absorption equivalent width threshold $W \gtrsim 0.3 \text{ \AA}$ (which corresponds to a neutral hydrogen column density threshold $N(\text{HI}) \gtrsim 1.3 \times 10^{14} \text{ cm}^{-2}$), we find that a typical L_* galaxy is surrounded by an extended gaseous halo of $\approx 180 h^{-1} \text{ kpc}$ radius with a covering factor of 94%.

4. Adopting the scaling relationship between the extent of tenuous gas around galaxies and galaxy B -band luminosity, we find that the predicted number density of Ly α absorption systems arising in extended gaseous halos of galaxies is equivalent to the comoving B -band luminosity density. Therefore, the observed number density evolution of Ly α absorption systems may serve to constrain the measurements of cosmic star formation rate density.

The authors thank the staff of STScI for their expert assistance and Sam Pascarella for helping to obtain some of the near-infrared images. This work was supported by STScI grant GO-07290.01-96A and NSF grant AST-9624216.

REFERENCES

- Bahcall, J. N. et al. 1993, ApJS, 87, 1
- _____. 1996, ApJ, 457, 19
- Barcons, X., Lanzetta, K. M., & Webb, J. K. 1995, Nature, 376, 321
- Bechtold, J. 1994, ApJS, 91, 1
- Bertin, E. & Arnouts, S. 1996, A&AS, 117, 393
- Bothun, G. D., Schombert, J. M., Impey, C. D., Sprayberry, D. & McGaugh, S. S. 1993, AJ, 106, 530
- Bowen, D. V., Blades, J. C., & Pettini, M. 1996, ApJ, 464, 141
- Bruzual, A. G. & Charlot, S. 1993, ApJ, 405, 538
- Chen, H.-W., Lanzetta, K. M., Webb, J. K., & Barcons, X. 1998, ApJ, 498, 77 (Paper I)
- Chen, H.-W., Lanzetta, K. M., & Fernández-Soto, A. 2000, ApJ, 533, 120
- Chen, H.-W. & Prochaska, J. X. 2000, ApJ, 543, L9
- Chen, H.-W., Lanzetta, K. M., & Webb, J. K. 2001, ApJ, in press
- Cowie, L. L., Songaila, A., Hu, E. M., & Cohen, J. G. 1996, AJ, 112, 839
- Cowie, L. L., Songaila, A., & Barger, A. J. 1999, AJ, 118, 603
- Dressler, A., Oemler, A., Couch, W. J., Smail, I., Ellis, R. S., Barger, A., Butcher, H., Poggianti, B. M., & Sharples, R. M. 1997, ApJ, 490, 577
- Ellingson, E. & Yee, H. K. C. 1994, ApJS, 92, 33
- Holmberg, E. 1975, in Galaxies and the Universe, ed. A. Sandage, M. Sandage, & J. Kristian (Chicago: Univ. Chicago Press), 123
- Impey, C. D., Petry, C. E., & Flint, K. P. 1999, ApJ, 524 536
- Lanzetta, K. M., Bowen, D. V., Tytler, D., & Webb, J. K. 1995, ApJ, 442, 538
- Lanzetta, K. M., Webb, J. K., & Barcons, X. 1995, in QSO Absorption Lines, ed. G. Meylan (Berlin: Springer-Verlag), p. 263
- _____. 1996, ApJ, 456, L17
- _____. 1997, in Proceedings of the 13th IAP Colloquium, Structure and Evolution of the Intergalactic Medium from QSO Absorption Line Systems, ed. P. Petitjean and S. Charlot, p. 213
- _____. 2001, in preparation

- Lanzetta, K. M., Wolfe, A. M., Altan, H., Barcons, X., Chen, H.-W., Fernández-Soto, A., Meyer, D. M., Ortiz-Gil, A., Savaglio, S., Webb, J. K., & Yahata, N. 1997, *AJ*, 114, 1337
- Le Brun, V., Bergeron, J., & Boissé, P. 1996, *A&A*, 306, 691
- Lilly, S. J., Le Fèvre, O., Hammer, F., & Crampton, D. 1996, *ApJ*, 461, 534
- Madau, P., Pozzetti, L., & Dickinson, M. 1998, *ApJ*, 498, 106
- Morris, S. L., Weymann, R. J., Smith, B. A., Terrile, R. J., Giovanelli, R., & Irwin, M. 1993, *ApJ*, 419, 524
- Ortiz-Gil, A., Lanzetta, K. M., Webb, J. K., Barcons, X., & Fernández-Soto, A. 1999, *ApJ*, 523, 720
- Pascarelle, S. M., Lanzetta, K. M., & Fernández-Soto 1998, *ApJ*, 508, L1
- Rauch, M. 1998, *AR&A*, 36, 267
- Shull, M. J., Stocke, J. T., & Penton, S. 1996, *AJ*, 111, 72
- Somerville, R. S. & Primack, J. R. 1999, in the Proceedings of the Xth Rencontre de Blois (astro-ph/9811001)
- Spinrad, H., Filippenko, A. V., Yee, H. K., Ellingson, E., Blades, J. C., Bahcall, J. N., Jannuzi, B. T., Bechtold, J., & Dobrzycki, A. 1993, *AJ*, 106, 1
- Steidel, C. C., Adelberger, K. L., Giavalisco, M., Dickinson, M., & Pettini, M. 1999, *ApJ*, 519, 1
- Stocke, J. T., Shull, J. M., Penton, S., Donahue, M., & Carilli, C. 1995, *ApJ*, 451, 24
- Tripp, T. M., Lu, L., & Savage, B. D. 1998, *ApJ*, 508, 200
- van Gorkom, J. 1993, in *The Evolution of Galaxies and Their Environmen*, Proc. 3d Tetons Summer Astrophysics Conference, ed. J. M. Shull & H. A. Thronsons, Jr., p. 345
- van Gorkom, J. H., Carilli, C. L., Stocke, J. T., Perlman, E. S., & Shull, J. M. 1996, *AJ*, 112, 1397
- Weymann et al. 1998, *ApJ*, 506, 1

Fig. 1.— Final images of galaxies obtained with HST using WFPC2 with the F702W. The spatial extent of each image is roughly $25 h^{-1}$ kpc on a side, and the orientation of each image is arbitrary.

Fig. 2.— Residuals of the W vs. ρ anti-correlation as a function of galaxy B -band luminosity L_B (the upper-left panel), redshift z (the upper-right panel), galaxy mean surface brightness $\langle\mu\rangle$ (the lower-left panel), and galaxy disk-to-bulge ratio D/B (the lower-right panel). Circles represent elliptical or S0 galaxies, triangles represent early-type spiral galaxies, and squares represent late-type spiral galaxies. Points with arrows indicate 3σ upper limits. The dotted line in the lower-left panel at $\langle\mu\rangle = 25.7$ indicates the borderline between low surface brightness and high surface brightness galaxies.

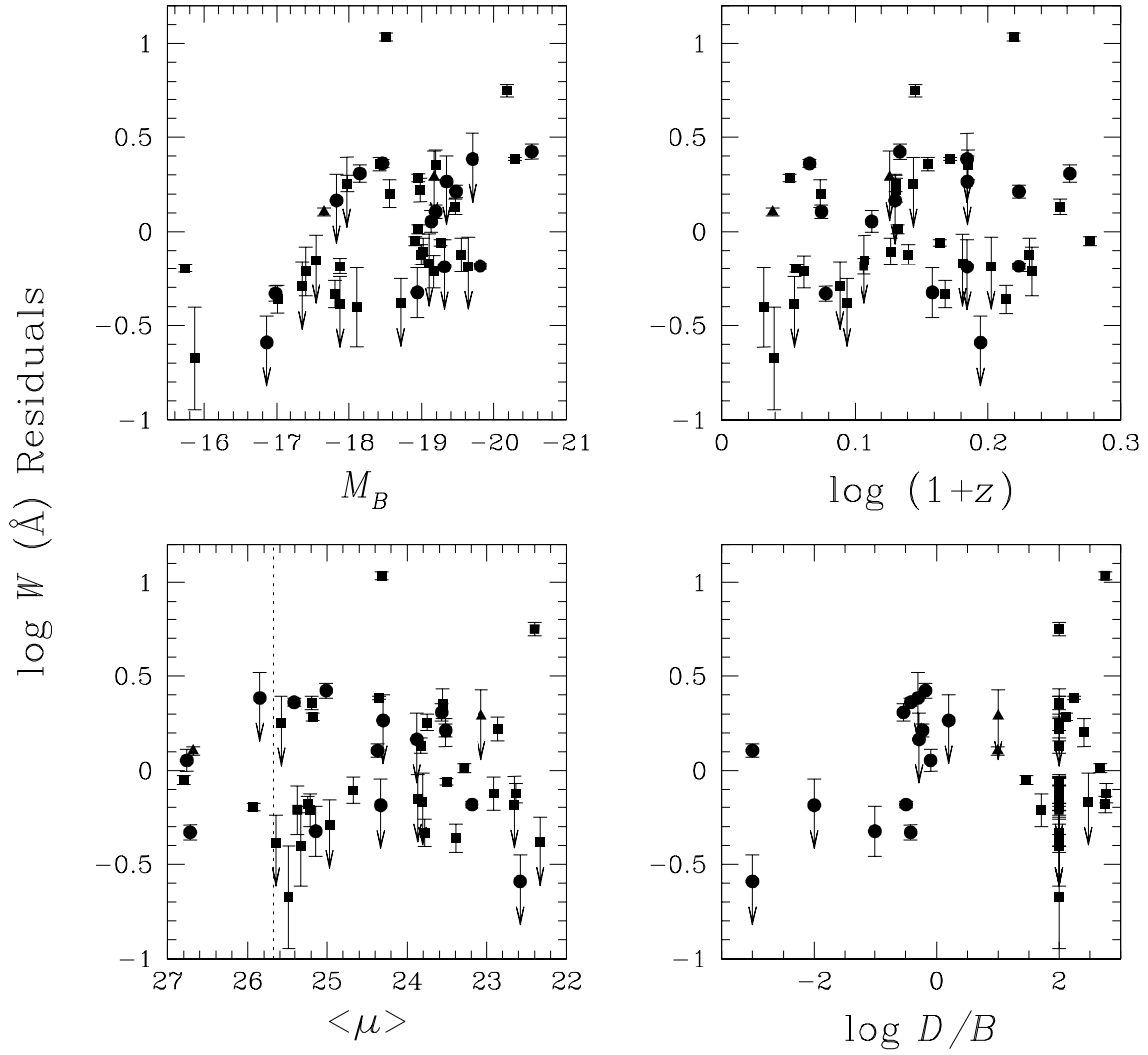
Fig. 3.— Logarithm of Ly α rest-frame equivalent width W vs. logarithm of galaxy impact parameter ρ . Symbols are the same as those in Figure 2. The cosmic scatter is indicated by the error bar in the upper-right corner.

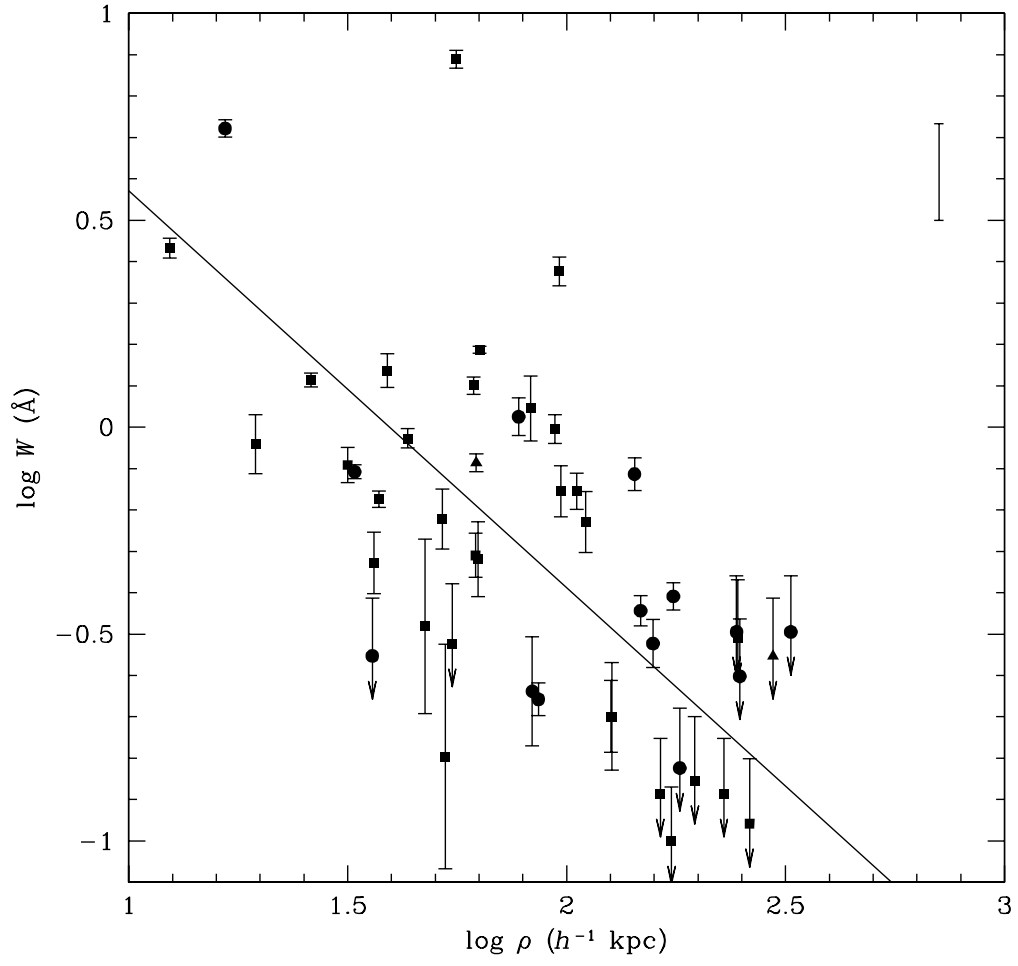
Fig. 4.— Logarithm of Ly α rest-frame equivalent width W vs. logarithm of galaxy impact parameter ρ scaled by galaxy B -band luminosity. The scaling factor is determined from the analysis described in §§ 6.1. Symbols are the same as those in Figure 2. The cosmic scatter is indicated by the error bar in the upper-right corner.

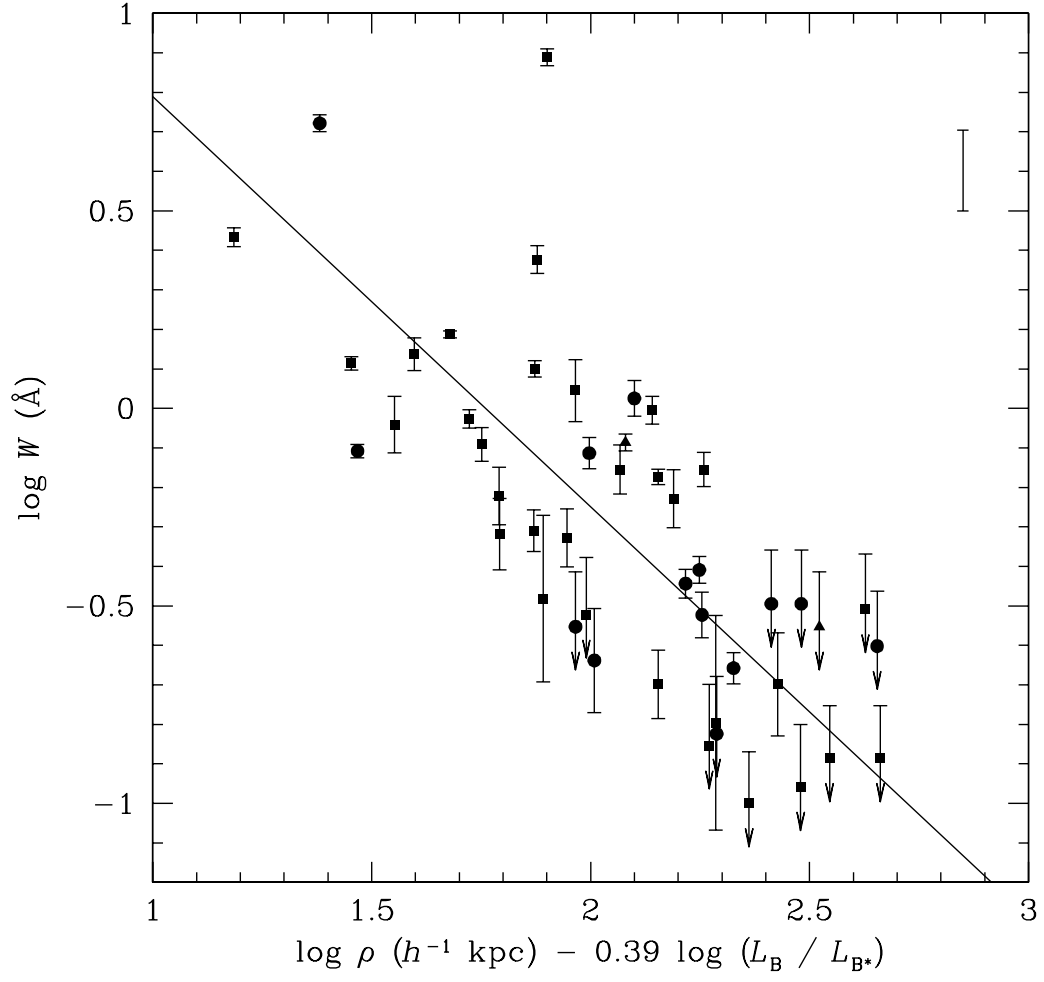
Fig. 5.— Logarithm of neutral hydrogen column density N vs. logarithm of galaxy impact parameter ρ scaled by galaxy B -band luminosity. The scaling factor is determined from the analysis described in §§ 6.1. Neutral hydrogen column densities are determined from Ly α rest-frame equivalent widths under the assumption that Doppler parameters are contained in the range $20 < b < 40$ km s $^{-1}$. Symbols are the same as those in Figure 2, and the cosmic scatter is indicated by the error bar in the upper-right corner.

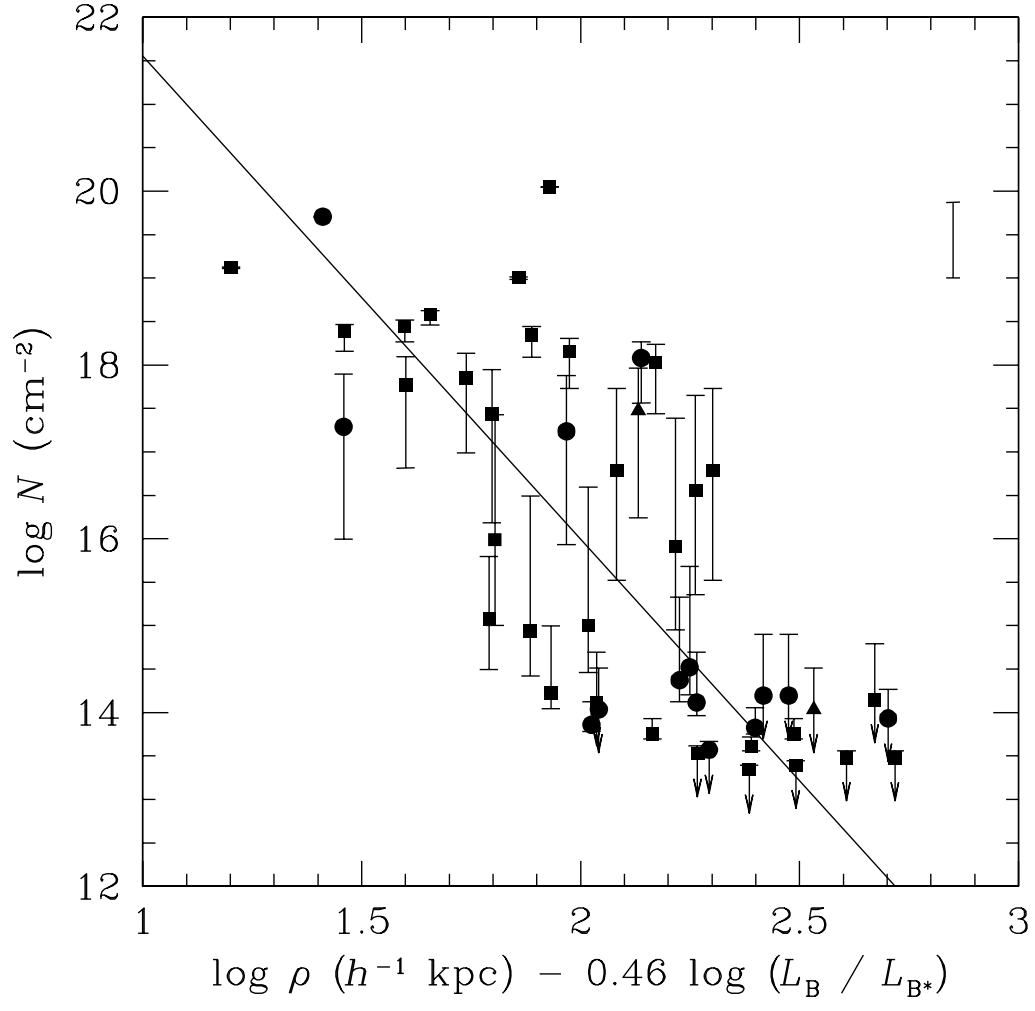
Fig. 6.— Comparison of the W vs. ρ anti-correlation scaled by galaxy K -band luminosity (the left panel) and by galaxy B -band luminosity (the right panel). The scaling factor is determined from the analysis described in §§ 6.1. Symbols are the same as those in Figure 2, and the cosmic scatter is indicated by the error bar in the upper-right corner.

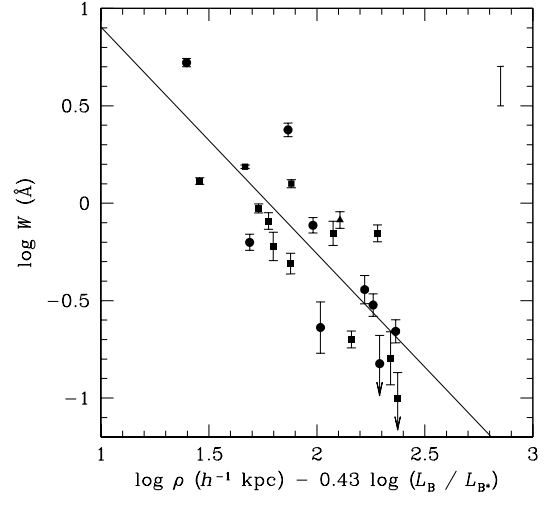
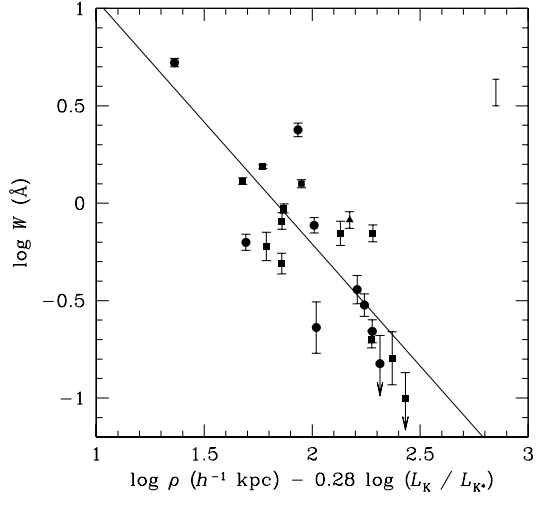
Fig. 7.— Galaxy K -band luminosity vs. galaxy B -band luminosity for galaxies in the sample with K -band photometric measurements available. Symbols are the same as those in Figure 2.











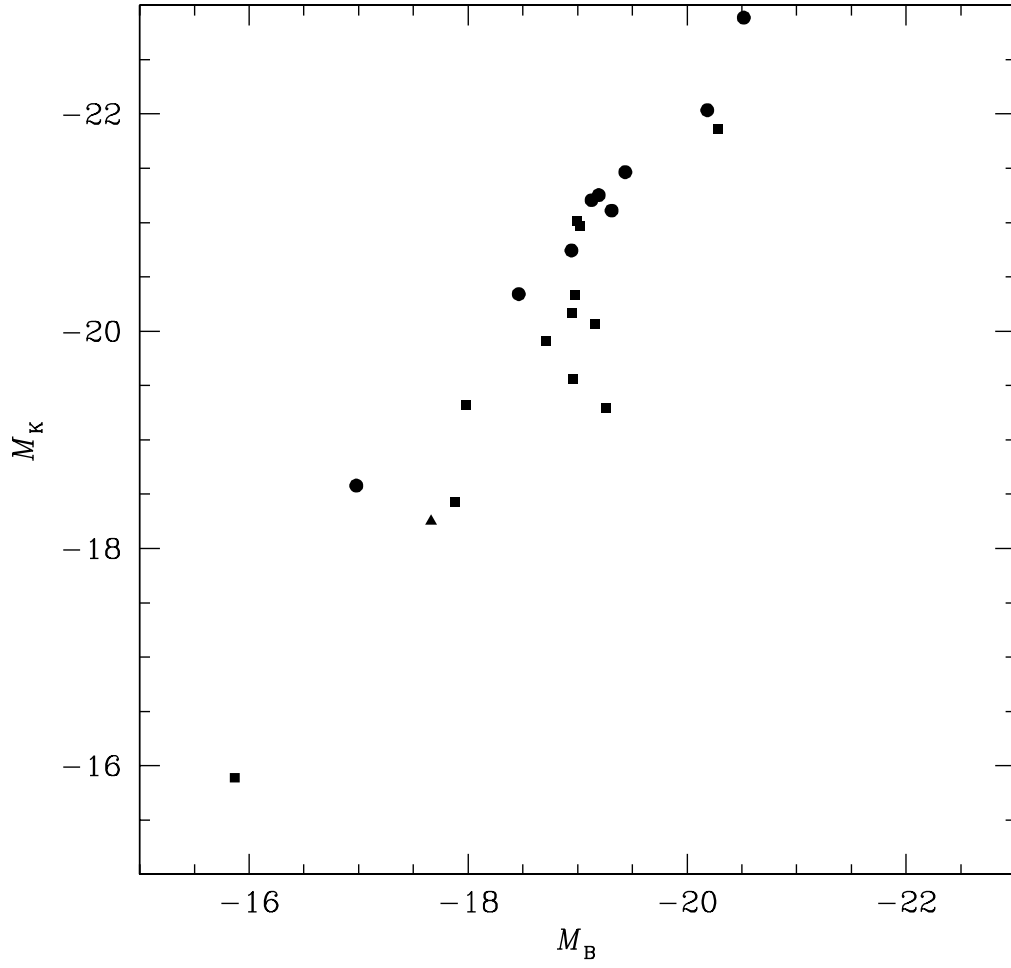


Table 1
Journal of Observations

Field	α (2000)	δ (2000)	z_{em}	Filter	Exposure	
					Time (s)	Date
0122–0021	01:25:28.8	–00:05:55.8	1.070	F702W	2100	3 Dec 1997
0405–1219	04:07:48.4	–12:11:36.0	0.574	F702W	2100	16 Sep 1998
0405–1219	04:07:48.4	–12:11:36.0	0.574	F702W	2100	23 Sep 1998
0903+1658	09:06:31.9	+16:46:11.5	0.412	F702W	2100	16 Nov 1997
1136–1334	11:39:10.7	–13:50:43.5	0.560	F702W	2100	10 Jun 1997
1216+0657	12:19:20.9	+06:38:38.4	0.331	F702W	2100	30 Mar 1998
1259+5920	13:01:12.9	+59:02:06.1	0.478	F702W	2100	20 Jan 1997
1259+5920	13:01:12.9	+59:02:06.1	0.478	F702W	2100	25 Oct 1998
1424–1150	14:27:38.2	–12:03:50.5	0.806	F702W	2100	7 Feb 1997
1641+3954	16:42:58.7	+39:48:36.0	0.593	F702W	2100	8 Sep 1998
2251+1552	22:53:57.7	+16:08:53.6	0.859	F702W	2100	6 Dec 1997

Table 2
Journal of Archival Observations

Field	α (2000)	δ (2000)	z_{em}	Filter	Exposure	
					Time (s)	Date
1317+2743	13:19:56.3	+27:28:08.4	1.022	F702W	4700	1 Jun 1995

Table 3
Summary of Other Observations

Field	Galaxies		Absorbers	
	Number Included	Reference	Number Included	Reference
0122–0021	4	1	3	1,2,3
0405–1219	15	1,4	5	1
0903+1658	13	1,4	0	1
1136–1334	13	1	0	1,2
1216+0657	5	1	1	1
1259+5920	4	1	1	1,2
1317+2743	4	5	2	1,2
1424–1150	7	1	1	1,2
1641+3954	15	4	1	1
2251+1552	1	1	1	1,2

REFERENCES—(1) our own observations and analysis, in preparation; (2) Bahcall et al. 1993; (3) Bahcall et al. 1996; (4) Ellingson & Yee 1994; (5) Le Brun, Bergeron, & Boissé 1996.

This figure "fig1a.gif" is available in "gif" format from:

<http://arxiv.org/ps/astro-ph/0107137v1>

This figure "fig1b.gif" is available in "gif" format from:

<http://arxiv.org/ps/astro-ph/0107137v1>

Table 4: Galaxies and Absorption Systems

Field (1)	Galaxies															Absorption Systems			
	$\Delta\alpha$ (arcsec) (2)	$\Delta\delta$ (arcsec) (3)	z_{gal} (4)	ρ (h^{-1} kpc) (5)	R_D (h^{-1} kpc) (6)	R_B (h^{-1} kpc) (7)	D/B (8)	α (deg) (9)	i (deg) (10)	b/a (11)	m_{WFPC2} (12)	$\langle\mu\rangle$ (13)	M_B $-5 \log h$ (14)	M_K $-5 \log h$ (15)	M_K $-5 \log h$ (16)	z_{abs} (17)	$W(\text{Ly}\alpha)$ (Å) (18)	$W(\text{CIV})$ (Å) (19)	
0122-0021	-8.7	-12.3	0.3788	47.1	2.3	0.3	> 50.0	49.5	48.0	0.54	20.6	23.3	-19.1	19.8	-20.4	0.3786	0.74	0.59	
	-16.8	24.8	0.3992	96.2	2.0	...	> 50.0	57.3	50.9	...	19.3	22.4	-20.2	18.3	-22.0	0.3989	2.38	1.70	
	40.7	-9.2	0.4299	138.9	1.2	...	> 50.0	20.1	62.8	...	21.9	23.1	-18.2	21.0	-19.4	0.4302	0.84	< 0.14	
	27.0	-37.2	0.3793	143.9	2.6	...	> 50.0	49.0	58.5	...	20.5	23.4	-19.2	19.7	-20.5	
0349-1438	-9.4	10.8	0.3567	43.4	2.4	0.9	> 50.0	156.2	43.1	0.13	20.6	23.3	-19.0	20.4	-19.6	0.3566	0.94	0.66	
	11.7	-24.1	0.3236	77.1	2.8	1.2	0.4	9.4	83.0	0.39	20.0	24.8	-18.9	18.4	-21.4	...	< 1.01	< 0.10	
	-29.2	18.3	0.3244	99.1	...	1.2	0.0	79.2	...	0.74	19.5	22.6	-19.4	18.1	-21.7	...	< 1.07	< 0.10	
	12.6	-45.9	0.2617	120.3	1.8	0.4	1.6	144.8	58.1	0.96	20.2	24.4	-18.2	18.8	-20.5	...	< 1.52	< 0.10	
0405-1219	-57.1	19.8	0.3273	174.8	3.1	...	> 50.0	9.9	57.6	...	20.2	23.6	-19.1	19.9	-20.0	...	< 0.79	< 0.09	
	7.3	3.6	0.5709	30.4	3.5	...	> 50.0	107.0	60.1	...	21.3	23.6	-19.5	20.2	-20.8	...	< 0.05	< 0.05	
	10.6	-6.7	0.5714	46.9	...	5.4	0.0	104.1	...	0.81	20.5	25.1	-20.1	19.1	-22.1	...	< 0.05	< 0.05	
	-3.3	-12.7	0.5696	49.0	18.5	-22.6	...	< 0.06	< 0.05	
	2.6	-15.0	0.5657	56.8	...	1.9	0.0	106.6	...	0.84	20.8	23.2	-19.8	19.3	-21.9	...	< 0.06	< 0.05	
	10.4	-26.9	0.5779	108.3	2.3	0.5	2.2	53.8	16.3	0.78	21.1	23.8	-19.6	19.3	-21.9	...	< 0.06	< 0.06	
	-1.4	33.9	0.1670	62.8	21.0	-17.3	0.1670	0.65	0.44	
	1.0	-35.0	0.3520	105.4	1.7	...	> 50.0	132.2	69.0	...	21.6	23.8	-18.0	20.6	-19.3	0.3514	0.70	< 0.10	
	14.0	-35.4	0.5777	143.0	1.9	0.4	1.4	95.8	70.9	0.83	21.5	23.9	-19.2	19.7	-21.6	...	< 0.06	< 0.06	
	40.5	-1.0	0.1668	74.9	16.6	-21.7	
	-37.2	28.4	0.3617	142.9	2.0	6.0	0.7	169.4	9.2	0.90	18.7	25.0	-20.5	17.2	-22.8	0.3610	0.77	0.15	
	16.1	-45.1	0.6167	183.9	3.1	...	> 50.0	176.3	56.0	...	21.8	23.7	-19.2	21.2	-20.1	
	-36.9	35.4	0.5696	191.1	4.0	0.7	4.9	122.3	67.5	0.94	20.6	24.3	-20.2	18.5	-22.7	...	< 0.06	< 0.05	
	31.9	-47.9	0.2973	157.4	3.3	6.4	0.8	26.8	62.8	0.98	19.5	26.8	-19.1	18.4	-21.2	0.2979	0.30	< 0.12	
	19.2	-70.0	0.5170	261.6	3.2	0.4	> 50.0	129.0	42.3	0.67	21.4	23.8	-19.1	< 0.11	< 0.08	
	-66.2	-30.9	0.1525	126.2	4.8	0.4	49.5	153.4	47.9	0.80	18.5	25.2	-19.2	18.1	-20.1	0.1532	0.20	< 0.17	
-65.6	56.7	0.2800	228.7	1.6	...	> 50.0	156.3	19.5	...	21.5	23.9	-17.5	< 0.13	< 0.11		
0454-2203	10.6	5.7	0.2784	31.6	3.4	0.1	> 50.0	102.5	70.3	0.91	21.1	25.2	-17.9	21.0	-18.4	0.2774	0.81	...	
	-1.1	-18.0	0.4847	63.3	7.1	0.3	> 50.0	83.8	42.6	0.79	20.1	24.4	-20.3	18.8	-21.9	0.4825	1.54	0.20	
	4.2	18.4	0.5325	68.8	...	1.0	0.0	44.3	...	0.43	21.8	22.7	-18.6	20.5	-20.5	...	< 0.04	< 0.08	
	0.3	-19.7	0.3818	61.9	1.6	0.1	> 50.0	114.3	47.2	0.62	20.8	22.6	-19.0	19.1	-21.0	0.3812	0.46	0.10	
	-18.2	42.9	0.4836	163.5	6.0	0.6	7.4	28.3	70.5	0.82	20.4	25.5	-19.9	18.5	-22.2	
	37.8	-36.5	0.4837	184.3	3.8	0.2	> 50.0	174.5	31.6	0.85	20.0	23.4	-20.4	
	35.6	-41.0	0.5336	198.3	7.3	1.4	> 50.0	129.9	75.7	0.54	21.1	25.2	-19.5	< 0.04	< 0.08	
	14.5	99.5	0.3382	296.2	1.6	0.2	10.0	110.5	44.7	0.82	20.2	23.1	-19.2	< 0.28	< 0.07	
0850+4400	-8.9	2.0	0.1635	16.6	1.4	2.5	0.4	128.3	55.9	0.64	18.7	25.4	-18.5	18.0	-20.3	0.1638	5.27	0.23	
	10.0	-2.4	0.4402	34.7	5.0	1.8	0.6	18.8	10.8	0.66	20.6	25.0	-19.2	19.6	-21.0	...	< 0.23	< 0.12	
	22.6	12.4	0.5007	92.9	3.2	0.1	> 50.0	14.3	61.0	0.86	20.9	24.5	-19.5	19.4	-21.4	...	< 0.10	< 0.17	
	3.4	35.0	0.0872	38.9	...	1.3	0.0	34.9	...	0.94	17.4	23.7	-18.3	16.6	-20.4	< 0.36	
	-0.5	40.5	0.0915	46.1	1.8	...	> 50.0	150.0	74.5	...	19.9	25.9	-16.5	20.1	-17.0	< 0.34	
	29.0	30.5	0.2766	110.1	2.5	...	> 50.0	56.7	11.6	...	20.9	24.2	-18.1	22.0	-17.5	< 0.19	
0903+1658	45.5	2.2	0.5196	164.6	...	2.4	0.0	86.2	...	0.88	20.1	23.1	-20.3	17.9	-23.1	...	< 0.09	< 0.18	
	6.6	-12.1	0.4106	44.9	3.3	1.0	11.2	38.4	48.3	0.25	19.8	23.9	-19.8	18.3	-22.0	...	< 0.09	< 0.06	
	4.0	-17.1	0.4258	58.2	4.4	...	> 50.0	3.3	82.8	...	21.8	25.6	-18.2	22.5	-17.9	
	-3.2	-24.0	0.4268	80.3	
	7.0	35.0	0.2690	91.8	
	-36.1	-12.2	0.2695	98.1	< 0.22	
	37.0	25.1	0.4100	145.5	1.8	2.0	0.2	150.5	29.4	0.77	20.5	24.4	-19.0	< 0.06	
	-17.8	47.1	0.2682	129.3	2.7	0.1	45.2	83.2	61.0	0.91	19.8	24.5	-19.0	18.1	-21.2	< 0.22	
	-39.8	33.8	0.4087	168.0	< 0.10	< 0.06
	-39.0	35.8	0.4094	172.2	< 0.09	< 0.06
	-28.1	51.3	0.2697	150.7	< 0.21
	-28.7	53.6	0.2702	156.8	< 0.21
-37.9	-50.6	0.4093	205.6	2.1	8.2	> 50.0	87.1	77.3	0.51	20.1	24.9	-19.5	18.6	-21.7	< 0.06		
-23.6	66.3	0.4115	229.4	2.4	...	> 50.0	55.5	53.3	...	21.1	23.5	-18.9	20.4	-19.9	...	< 0.10	< 0.06		

Table 4: — Continued

Field (1)	Galaxies														Absorption Systems			
	$\Delta\alpha$ (arcsec) (2)	$\Delta\delta$ (arcsec) (3)	z_{gal} (4)	ρ (h^{-1} kpc) (5)	R_D (h^{-1} kpc) (6)	R_B (h^{-1} kpc) (7)	D/B (8)	α (deg) (9)	i (deg) (10)	b/a (11)	m_{WFPC2} (12)	$\langle\mu\rangle$ (13)	$-5 \log h$ (14)	m_K (15)	$-5 \log h$ (16)	z_{abs} (17)	$W(\text{Ly}\alpha)$ (Å) (18)	$W(\text{CIV})$ (Å) (19)
1001+2910	-3.4	-23.1	0.1380	37.6	1.8	...	> 50.0	168.8	68.3	...	21.7	25.9	-15.7	0.1377	0.67	< 0.12
	-28.4	6.6	0.3308	85.0	1.1	1.0	0.9	96.6	66.6	0.79	20.5	23.1	-18.4	< 0.18	< 0.05
	13.4	-61.8	0.2143	140.1	1.8	3.9	3.4	168.3	33.3	0.26	21.7	25.3	-16.6	0.2130	0.57	< 0.11
1136-1334	-14.4	-9.5	0.3191	49.2	3.1	0.4	29.2	40.6	73.8	0.73	20.5	25.7	-18.9	19.2	-20.5	0.3189	...	0.22
	0.4	23.3	0.5550	86.3	19.8	< 0.06	< 0.10
	10.8	-25.5	0.2044	59.4	2.4	...	> 50.0	1.4	74.8	...	20.0	24.1	-18.3	18.2	-20.6	0.76
	-36.5	-1.2	0.2198	82.3	0.7	0.1	3.2	155.9	51.1	0.61	22.3	25.2	-15.6	21.3	-17.7	< 0.08
	1.9	-37.1	0.6480	144.8	2.2	0.5	1.4	112.1	53.6	0.80	21.3	23.1	-19.9	19.8	-21.7
	44.2	9.1	0.5575	167.4	0.5	1.4	0.0	49.0	79.2	0.27	22.3	23.7	-18.3	< 0.06	< 0.10
	-18.2	-48.3	0.2123	113.6	1.6	0.5	3.2	98.0	76.8	1.00	20.0	24.6	-18.3	18.5	-20.4	< 0.13
	-52.0	13.8	0.3598	163.8	9.6	0.8	4.2	6.3	71.4	0.79	19.2	25.9	-20.4	17.4	-22.6	< 0.13
	-3.2	55.7	0.1755	107.2	19.8	< 0.22
	17.8	-54.2	0.4007	183.6	4.2	...	> 50.0	34.9	64.2	...	21.1	24.6	-18.8	20.5	-19.7	< 0.24
	-27.1	51.5	0.3604	177.4	0.6	...	> 50.0	99.5	54.2	...	21.5	21.8	-18.1	19.9	-20.1	< 0.35
	-45.1	38.8	0.3595	181.1	2.8	2.6	0.4	6.8	13.5	0.84	19.1	23.2	-20.0	17.2	-22.9	< 0.13
	-7.3	-80.7	0.3254	233.5	3.1	...	> 50.0	119.8	40.5	...	19.5	23.0	-19.9	< 0.15
1216+0655	37.2	-18.8	0.1242	61.3	4.4	0.7	> 50.0	104.3	51.6	0.54	18.2	25.2	-19.0	17.6	-20.2	0.1243	1.26	0.31
	-16.9	-56.9	0.6021	226.1	4.0	...	> 50.0	50.2	53.5	...	21.0	23.4	-20.0	19.8	-21.4
	-18.6	-89.3	3.2720	320.4	0.3	1.8	0.4	1.3	54.8	0.89	21.6	16.4	-28.0
	49.6	-77.5	0.4341	307.7	1.6	0.7	5.5	11.1	70.6	0.80	21.2	24.2	-18.9
	-60.6	-77.4	0.0012	1.7	...	0.0	0.0	81.5	...	0.93	21.5	25.0	-4.8
1259+5920	27.0	-31.3	0.1967	86.2	0.9	2.0	0.4	135.1	74.9	0.76	20.6	26.7	-17.0	20.1	-18.6	0.1966	0.22	< 0.16
	-60.5	3.9	0.5353	221.5	3.7	...	> 50.0	52.9	67.8	...	21.1	23.7	-19.5
	-23.4	68.5	0.2412	173.6	1.3	...	> 50.0	106.2	29.4	...	20.0	22.3	-18.7	19.2	-19.9	...	< 0.10	< 0.15
	8.7	110.9	0.4869	391.3	1.7	...	> 50.0	25.5	30.9	...	21.1	22.3	-19.3	19.9	-20.8
1317+2743	6.8	4.8	0.6715	32.8	2.4	1.7	0.3	29.3	63.9	0.98	21.5	23.2	-19.8	0.6716	0.78	...
	-44.4	-2.3	0.6717	175.2	2.7	1.5	0.6	9.8	13.7	0.93	21.8	23.5	-19.5	0.6736	0.39	< 0.14
	-66.1	10.5	0.5397	245.3	< 0.10	...
	-68.1	9.7	0.5398	252.1	< 0.10	...
1354+1933	1.2	7.5	0.4592	26.1	3.1	...	> 50.0	67.7	25.6	...	21.0	23.5	-19.3	21.3	-19.3	0.4569	1.41	0.89
	-21.6	-12.2	0.4406	83.5	0.6	3.2	0.1	68.1	67.8	0.84	20.9	25.1	-18.9	19.9	-20.7	0.4412	0.23	< 0.11
	-16.0	-23.3	0.4295	94.1	4.2	...	> 50.0	20.9	79.3	...	21.6	25.2	-18.4	0.4307	1.03	< 0.11
	-13.4	-48.0	0.5293	181.3	0.1	2.6	0.0	57.9	1.8	0.86	21.1	24.3	-19.3	19.9	-21.1	...	< 0.15	< 0.24
	65.8	50.1	0.3509	248.5	1.0	6.5	0.5	45.3	73.2	0.78	21.3	23.9	-17.8	< 0.25	< 0.05
1424-1150	3.0	-1.3	0.8011	13.4	2.4	...	> 50.0	33.7	55.1	...	22.2	22.8	-19.7	< 0.04	< 0.11
	-0.2	17.6	0.3404	52.0	4.7	...	> 50.0	178.7	76.5	...	20.5	24.7	-19.0	18.9	-21.0	0.3417	0.60	< 0.16
	-11.4	40.9	0.1064	55.0	0.7	...	> 50.0	62.2	27.7	...	21.7	24.7	-15.1	< 0.38
	-69.1	-33.9	0.3942	245.7	4.1	...	> 50.0	104.8	74.3	...	21.9	25.6	-18.0	< 0.31	< 0.31
	-17.8	86.4	0.1038	111.9	0.7	1.1	0.1	147.9	77.5	0.80	18.8	24.5	-17.3	17.8	-19.6	< 0.34
	-88.1	-47.8	0.1045	127.9	1.9	1.5	4.5	172.3	47.3	0.75	19.3	24.9	-17.3
	-91.3	-53.8	0.2597	266.6	1.7	1.9	8.1	82.0	54.9	0.48	20.3	25.6	-18.4	< 0.24
1545+2101	-2.7	-1.1	0.2657	7.2	0.3	2.6	0.0	36.4	75.4	0.91	19.9	24.3	-19.1	0.2641	0.63	< 0.16
	16.6	-8.7	0.2639	47.6	2.8	2.1	2.2	161.2	20.6	0.80	19.5	23.5	-19.4	17.9	-21.5	< 0.16
	-26.3	23.1	0.1343	55.1	4.2	...	> 50.0	171.0	80.8	...	19.7	25.6	-17.9	< 0.30	< 0.38
	27.3	-35.6	0.0949	53.4	1.8	...	> 50.0	173.4	54.7	...	20.9	25.5	-15.9	21.3	-15.9	0.0961	0.16	< 0.57
1622+2352	-1.5	2.1	0.9310	10.9	2.6	0.5	13.1	93.5	69.4	0.94	24.0	24.2	-18.6	< 0.08	< 0.07
	3.0	-0.0	0.8920	12.4	4.2	0.8	28.6	124.1	80.0	0.54	23.3	26.8	-18.9	0.8909	2.71	0.91
	-4.2	-3.8	0.4720	19.5	1.3	...	> 50.0	96.8	74.0	...	22.5	23.8	-17.8	0.4716	0.91	0.52
	-5.5	7.5	0.6350	36.3	0.7	...	> 50.0	123.5	56.2	...	24.1	23.4	-17.0	0.6359	0.47	< 0.18
	-8.9	3.2	0.7980	39.0	3.8	...	> 50.0	63.6	65.6	...	22.4	23.8	-19.5	0.7964	1.37	1.38
	-3.3	9.1	0.5650	36.0	...	0.2	0.0	115.0	...	0.64	23.8	22.6	-16.9	< 0.28	< 0.20
	-1.3	11.3	0.9210	47.9	0.4	4.0	0.0	12.1	64.3	0.93	22.2	23.7	-20.6	< 0.09	< 0.08

Table 4: — Continued

Field (1)	Galaxies														Absorption Systems			
	$\Delta\alpha$ (arcsec) (2)	$\Delta\delta$ (arcsec) (3)	z_{gal} (4)	ρ (h^{-1} kpc) (5)	R_D (h^{-1} kpc) (6)	R_B (h^{-1} kpc) (7)	D/B (8)	α (deg) (9)	i (deg) (10)	b/a (11)	m_{WFPC2} (12)	$\langle\mu\rangle$ (13)	$-5 \log h$ (14)	m_K (15)	$-5 \log h$ (16)	z_{abs} (17)	$W(\text{Ly}\alpha)$ (Å) (18)	$W(\text{CIV})$ (Å) (19)
	-6.7	9.7	0.3180	33.6	2.6	3.3	0.9	58.6	72.0	0.75	20.2	26.5	-18.6	...	0.3174	...	0.78	
	-11.1	-4.3	1.0370	51.0	2.5	...	> 50.0	37.3	56.1	...	23.7	23.3	-19.1	
	-5.1	11.1	0.9200	51.4	0.5	2.4	0.8	53.5	61.4	0.45	23.8	22.2	-19.1	< 0.09	< 0.08	
	7.3	-12.1	0.9200	59.5	7.2	0.3	> 50.0	147.6	18.6	0.36	21.8	23.5	-20.6	< 0.09	< 0.08	
	1.6	14.2	0.6560	55.9	3.1	0.2	> 50.0	87.7	54.7	0.42	22.7	24.3	-18.5	...	0.6564	7.75	0.33	
	-12.3	9.9	0.7020	62.8	2.5	0.1	> 50.0	114.7	36.7	0.34	21.9	22.9	-19.5	...	0.7020	0.48	...	
	18.2	0.2	1.0100	77.7	2.1	...	> 50.0	82.5	70.6	...	24.9	24.5	-17.8	
	7.9	-17.0	0.8280	77.7	0.5	0.6	0.3	169.6	58.1	0.73	24.2	23.6	-18.1	...	0.8273	1.06	< 0.15	
	-21.3	-6.2	0.3680	68.4	2.8	...	> 50.0	91.7	58.3	...	19.9	22.8	-19.8	
	-24.1	5.3	0.3680	75.9	1.2	...	> 50.0	96.5	74.7	...	23.4	25.2	-16.2	
	15.0	19.6	1.0180	105.2	
	8.8	-24.8	0.9190	111.0	4.4	...	> 50.0	130.6	51.3	...	22.4	23.5	-20.0	< 0.09	< 0.09	
	-26.4	-2.7	0.9240	111.8	0.3	2.4	0.0	33.1	61.5	0.85	22.7	23.3	-20.2	< 0.08	< 0.08	
	-28.9	5.7	0.9230	124.1	1.5	...	> 50.0	172.5	60.5	...	24.3	23.6	-18.1	< 0.09	< 0.08	
	25.5	17.6	0.2610	78.1	1.6	1.0	4.8	48.2	56.2	0.47	21.6	25.1	-17.1	
	-7.9	30.7	0.7090	126.7	2.2	...	> 50.0	95.9	80.2	...	24.0	25.4	-17.4	0.20	< 0.18	
	12.7	-31.2	0.2800	88.9	0.3	0.5	0.0	112.4	84.7	0.63	22.9	26.0	-15.6	< 0.27	
	-34.3	3.2	1.0110	146.9	...	6.5	0.0	163.0	...	0.98	21.9	24.5	-21.4	
	-7.6	-43.4	0.8920	184.6	2.0	...	> 50.0	5.6	31.5	...	23.8	23.5	-18.5	
	-45.4	7.7	0.6680	181.1	2.1	...	> 50.0	13.4	65.3	...	24.4	25.4	-16.9	
	-46.8	7.7	0.6380	183.9	3.5	...	> 50.0	0.6	81.8	...	24.9	26.8	-16.2	
1641+3954	6.8	-1.3	0.5880	26.2	1.8	...	> 50.0	9.7	27.6	...	21.2	22.2	-19.6	< 0.17	< 0.20	
	12.2	-18.9	0.2813	59.5	1.2	...	> 50.0	136.5	58.6	...	22.7	24.6	-16.3	< 0.28	
	-16.4	-15.7	0.5319	82.7	2.8	...	> 50.0	118.6	66.9	...	21.4	23.6	-19.2	...	0.5342	1.11	< 0.38	
	-20.8	10.7	0.4126	76.4	1.6	...	> 50.0	82.7	41.2	...	21.5	23.1	-18.4	< 0.42	< 0.21	
	-10.8	27.9	0.5900	113.2	1.7	...	> 50.0	44.4	34.4	...	21.4	22.2	-19.5	< 0.16	< 0.20	
	28.9	-36.9	0.5918	177.5	4.7	1.5	8.2	74.5	71.3	0.91	21.0	25.2	-19.9	< 0.14	< 0.18	
	-36.6	36.6	0.5934	196.2	2.0	...	> 50.0	78.7	47.4	...	21.2	22.6	-19.6	< 0.14	< 0.18	
	-44.1	32.3	0.6944	217.4	2.1	...	> 50.0	16.2	34.6	...	21.1	21.8	-20.3	
	40.6	-38.8	0.3316	163.6	1.4	2.3	2.5	21.7	45.4	0.92	20.8	25.4	-18.5	< 1.48	< 0.32	
	-50.6	-32.7	0.4055	195.0	1.5	1.8	1.0	52.0	26.3	0.75	21.0	24.7	-18.5	< 0.47	< 0.24	
	-62.1	6.5	0.5917	236.5	3.6	...	> 50.0	66.2	39.0	...	21.3	23.7	-19.6	< 0.14	< 0.18	
	-18.3	64.6	0.5296	244.3	3.2	0.9	1.6	0.8	54.9	0.80	21.1	24.3	-19.3	< 0.32	< 0.39	
	32.2	62.5	0.2410	168.5	2.6	1.5	> 50.0	155.5	53.8	0.12	21.3	25.1	-17.3	< 0.29	
	25.6	-66.8	0.2192	160.9	1.9	0.5	> 50.0	23.6	62.4	0.84	22.4	25.8	-16.1	< 0.43	
1704+6048	32.1	-83.4	0.5289	325.0	0.9	5.2	0.5	114.0	42.7	0.65	20.7	25.9	-19.7	< 0.32	< 0.38	
	8.1	-27.1	0.3615	86.4	2.9	...	> 50.0	50.5	61.3	...	20.6	23.6	-19.1	20.4	-19.7	0.3621	0.49	< 0.09
	-31.3	-9.4	0.3380	96.2	3.2	...	> 50.0	43.3	58.6	...	21.5	24.9	-18.0	19.9	-20.0	...	< 0.52	< 0.13
	-14.2	-30.4	0.0713	30.8	0.7	...	> 50.0	46.9	78.9	...	21.8	25.8	-14.1	
	26.8	-35.2	0.3731	136.9	...	3.3	0.0	87.2	...	0.63	19.6	23.8	-19.7	17.5	-22.7	0.3716	0.26	< 0.08
	-51.0	18.3	0.0921	62.2	3.7	0.7	9.9	48.6	69.6	0.93	18.7	26.7	-17.7	18.9	-18.3	0.0920	0.82	< 0.16
	54.4	10.2	0.4033	178.7	1.9	...	> 50.0	168.8	60.8	...	21.5	23.6	-18.4	21.1	-19.1
	-70.0	13.3	0.2260	163.6	2.5	0.1	> 50.0	159.3	43.0	0.58	21.2	25.0	-17.4	< 0.13	< 0.20	
	72.9	5.9	0.1877	147.4	0.4	2.9	0.0	58.3	89.8	0.78	18.3	24.4	-19.2	17.4	-21.3	0.1880	0.36	< 0.21
2135-1446	4.7	-2.6	0.1996	11.3	2.5	1.5	1.0	91.4	78.7	0.66	19.6	24.7	-18.5	...	0.2005	1.80	0.85	
	-7.3	15.7	0.2000	36.6	...	1.3	0.0	36.3	...	0.48	19.2	22.6	-19.0	
	13.1	-21.7	0.1986	53.3	1.6	1.3	> 50.0	117.0	54.7	0.01	20.4	24.3	-18.0	
	18.6	-33.5	0.1991	80.8	2.5	1.4	4.3	154.5	39.5	0.39	20.0	24.4	-18.5	
	28.4	-31.3	0.2011	89.6	2.8	...	> 50.0	22.3	54.3	...	18.3	23.1	-20.2	
	-0.8	49.3	0.0752	47.8	4.6	...	> 50.0	33.2	73.6	...	18.1	25.3	-18.1	0.0750	0.33	< 0.39
	50.8	-21.7	0.1857	111.0	2.1	0.0	> 50.0	37.5	68.2	0.66	19.8	23.5	-18.6	0.1861	0.59	< 0.14
2251+1552	32.2	-0.3	0.3529	97.0	1.9	...	> 50.0	96.8	29.4	...	20.6	22.9	-19.0	19.6	-20.3	0.3526	0.70	< 0.16

Table 2.5: Results of Statistical Tests

Measurements	$a/\delta a$	Generalized								
		Kendall		Kendall		Spearman		Pearson		σ_c
		r_{gk}	r_{gk}/σ_{gk}	r_k	r_k/σ_k	r_s	r_s/σ_s	r_p	r_p/σ_p	
1. $W - \rho$	8.7	-0.44	-4.73	-0.43	-4.25	-0.61	-4.13	-0.63	-5.33	0.233
2. $W - \rho - L_B$	10.4,4.6	-0.58	-5.91	-0.57	-5.60	-0.77	-5.23	-0.73	-7.06	0.204
3. $W - \rho - r_e$	10.0,4.1	-0.48	-4.91	-0.45	-4.50	-0.65	-4.40	-0.67	-5.91	0.224
4. $W - \rho - \langle \mu \rangle$	8.2,0.9	-0.47	-4.80	-0.43	-4.30	-0.61	-4.15	-0.63	-5.31	0.236
5. $W - \rho - D/B$	8.6,1.7	-0.47	-4.76	-0.42	-4.19	-0.62	-4.20	-0.63	-5.37	0.257
6. $W - \rho - (1+z)$	8.5,3.2	-0.50	-5.06	-0.47	-4.65	-0.66	-4.50	-0.65	-5.63	0.224
7. $W - R$	7.4	-0.38	-3.82	-0.35	-3.42	-0.51	-3.43	-0.49	-3.73	0.250
8. $W \cos i - R$	8.9	-0.37	-3.79	-0.34	-3.35	-0.47	-3.18	-0.51	-3.97	0.243
9. $W \cos i - R - L_B$	11.1,6.7	-0.52	-5.36	-0.51	-5.03	-0.70	-4.71	-0.68	-6.20	0.151
10. $W \cos i - R - r_e$	9.2,2.8	-0.38	-3.87	-0.35	-3.42	-0.46	-3.14	-0.53	-4.17	0.240
11. $W \cos i - R - \langle \mu \rangle$	15.6,12.3	-0.35	-3.52	-0.33	-3.26	-0.49	-3.35	-0.51	-3.95	0.248
12. $W \cos i - R - D/B$	8.2,1.1	-0.37	-3.73	-0.33	-3.24	-0.46	-3.12	-0.51	-3.93	0.251
13. $W \cos i - R - (1+z)$	9.7,4.3	-0.42	-4.32	-0.40	-3.95	-0.56	-3.78	-0.57	-4.56	0.239
14. $N - \rho$	11.2	-0.46	-4.73	-0.43	-4.25	-0.61	-4.13	-0.63	-5.38	1.216
15. $N - \rho - L_B$	13.2,6.0	-0.57	-5.82	-0.56	-5.53	-0.77	-5.23	-0.74	-7.22	0.872
16. $N - \rho - r_e$	11.7,3.7	-0.49	-4.97	-0.46	-4.58	-0.65	-4.42	-0.67	-5.94	1.121
17. $N - \rho - \langle \mu \rangle$	10.9,0.0	-0.46	-4.73	-0.43	-4.25	-0.61	-4.13	-0.63	-5.38	1.200
18. $N - \rho - D/B$	9.3,2.1	-0.48	-4.84	-0.43	-4.26	-0.64	-4.32	-0.64	-5.58	1.371
19. $N - \rho - (1+z)$	11.7,3.7	-0.50	-5.05	-0.47	-4.65	-0.66	-4.51	-0.65	-5.69	1.270
20. $N - R$	9.4	-0.38	-3.86	-0.35	-3.46	-0.51	-3.44	-0.49	-3.77	1.432
21. $N \cos i - R$	10.4	-0.38	-3.89	-0.36	-3.55	-0.50	-3.41	-0.51	-3.93	1.266
22. $N \cos i - R - L_B$	16.1,7.5	-0.46	-4.66	-0.45	-4.50	-0.63	-4.26	-0.60	-5.00	1.449
23. $N \cos i - R - r_e$	10.3,3.4	-0.41	-4.13	-0.37	-3.71	-0.53	-3.62	-0.55	-4.39	0.971
24. $N \cos i - R - \langle \mu \rangle$	9.3,0.4	-0.37	-3.81	-0.35	-3.46	-0.49	-3.33	-0.51	-3.92	1.347
25. $N \cos i - R - D/B$	9.9,3.0	-0.38	-3.89	-0.34	-3.35	-0.49	-3.36	-0.54	-4.31	1.555
26. $N \cos i - R - (1+z)$	11.3,4.6	-0.42	-4.24	-0.40	-3.99	-0.57	-3.89	-0.56	-4.52	1.336

Table 2.6: Statistical Tests of The K Selected Sample

Measurements	$a/\delta a$	Generalized								
		Kendall		Kendall		Spearman		Pearson		σ_c
		r_{gk}	r_{gk}/σ_{gk}	r_k	r_k/σ_k	r_s	r_s/σ_s	r_p	r_p/σ_p	
1. $W - \rho$	6.6	-0.43	-2.79	-0.42	-2.74	-0.56	-2.59	-0.64	-3.64	0.223
2. $W - \rho - L_K$	7.0,4.4	-0.58	-3.81	-0.58	-3.81	-0.74	-3.40	-0.81	-5.94	0.136
3. $W - \rho - L_B$	6.9,4.4	-0.62	-4.00	-0.62	-4.03	-0.79	-3.63	-0.81	-5.97	0.202
4. $W - \rho - (B - K)$	5.8,3.0	-0.47	-3.08	-0.62	-4.03	-0.60	-2.73	-0.72	-4.50	0.264

Table 6: Statistical Tests of The K Selected Sample

Measurements	$a/\delta a$	Generalized		Kendall		Spearman		Pearson		σ_c
		Kendall		r_k	r_k/σ_k	r_s	r_s/σ_s	r_p	r_p/σ_p	
		r_{qk}	r_{qk}/σ_{qk}							
1. $W - \rho$	6.6	-0.43	-2.79	-0.42	-2.74	-0.56	-2.59	-0.64	-3.64	0.223
2. $W - \rho - L_K$	7.0,4.4	-0.58	-3.81	-0.58	-3.81	-0.74	-3.40	-0.81	-5.94	0.136
3. $W - \rho - L_B$	6.9,4.4	-0.62	-4.00	-0.62	-4.03	-0.79	-3.63	-0.81	-5.97	0.202